AIAA JOURNAL
Vol. 46, No. 3, March 2008

Flow and Noise Predictions for Single and Dual-Stream Beveled Nozzles

K. Viswanathan*
The Boeing Company, Seattle, Washington 98124-2207
M. Shur†
New Technologies and Services, 197198 St. Petersburg, Russia
P. R. Spalart‡
The Boeing Company, Seattle, Washington 98124-2207
and
M. Strelets§
New Technologies and Services, 197198 St. Petersburg, Russia

DOI: 10.2514/1.27299

Numerical simulations of the flowfield and noise of single and staggered dual, round, and beveled nozzles are carried out, with the goal of gaining insights into the flow features that are responsible for noise generation and mitigation, and ultimately arriving at better designs. For aircraft applications, the geometry of the nozzles must be satisfactory both for aerodynamic and acoustic performance. The importance of taking the nozzle internal flow into account in the simulations instead of using simple inflow profiles, especially for complex geometries of current interest, is emphasized. A two-step Reynolds-averaged Navier–Stokes/large-eddy simulation methodology is developed and applied to several nozzle geometries, allowing a new level of complexity in the geometry. The predictions of the gross thrust measures by Reynolds-averaged Navier–Stokes computations are in very good agreement with experimental measurements. The spectral predictions from large-eddy simulation are also in good agreement with measured data, for a wide range of jet conditions. The measured azimuthal variations in the noise field from beveled nozzles are reproduced by large-eddy simulation. The spectra from dual-stream nozzles are also well predicted. Preliminary efforts at establishing the link between flow and noise are presented. The interpretation of the flow/noise connection is not straightforward and is a big challenge; it is far from clear how one can establish cause and effect. The ability to relate changes in flow to noise may remain an open issue for the foreseeable future.

I. Introduction

THERE has been significant research effort in the last two decades to obtain a better understanding of the sources of jet noise, so as to enable the development of noise reduction concepts. The generation and propagation characteristics of turbulent mixing noise are neither well understood nor predicted to the level of accuracy needed, if only because of the shortcomings in the description of the underlying turbulent jet flows. Consequently, there is a heavy reliance on experimental measurements, both for flow and far-field noise. Given the lack of a quantitative method for relating the changes in flow, say due to changes in the nozzle geometry, to noise, the development of noise reduction concepts has remained an art based on heuristic thinking and experience rather than on physics and first principles. The prevailing state of knowledge perhaps explains the absence of any recent quantum step for jet noise reduction, despite substantial research. Further increases in bypass ratio now conflict with aircraft performance. For aircraft applications, any noise reduction design must meet stringent requirements on the impact on propulsive performance. Excessive and unacceptable thrust loss has rendered many potential nozzle configurations unsuitable; other concepts lower noise over a certain frequency range, but raise it over another range. This state of affairs motivates systematic research into all promising concepts, such as that of beveling the nozzles.

Detailed measurements of the characteristics of the time-dependent turbulent flow are extremely difficult or impossible in some cases. Numerical simulations, on the other hand, can provide information on the entire flowfield, albeit with limitations on accuracy, as always when turbulence is involved. The advances in computers have facilitated the application of large-eddy simulation (LES) for geometries of interest to the jet aeroacoustics community; several research groups have adopted this approach for flow/noise computations, see [1–12] for a partial list. The advantages and the disadvantages of several choices within the development of a numerical system for noise prediction using LES have been examined in detail by Shur et al. [1–3]. These include justifications and rationales for the different choices for the grid topology, the discretization scheme, the boundary conditions, the use/disabling of a subgrid scale model, etc., adopted in the prediction procedure. Along with that, validation studies for many test cases from a variety of nozzle geometries and a comprehensive list of references are reported in these three papers.

The developed numerical system, with recent improvements, is used here to carry out simulations of jets from beveled nozzles studied experimentally by Viswanathan in [13–15]. In particular, detailed measurements of the noise and the thrust of beveled nozzles from single jets [13] demonstrated significant noise benefit relative to a round nozzle in the peak noise radiation sector. Some of the salient acoustic characteristics of the beveled nozzle are summarized first. The beveled nozzles introduce significant azimuthal variations in the spectra. The spectral shapes at different azimuthal angles for a given

Presented as Paper 2445 at the 12th AIAA/CEAS Aeroacoustics Conference, Boston, MA, 8–10 May 2006; received 14 August 2006; revision received 15 March 2007; accepted for publication 15 October 2007.

*Associate Technical Fellow, Aeroacoustics and Fluid Mechanics; k.viswanathan@boeing.com. Associate Fellow AIAA.
†Leading Research Scientist; mshur@rscac.spb.ru. Senior Member AIAA.
‡Senior Technical Fellow, Aeroacoustics and Fluid Mechanics; philippe.r.spalart@boeing.com.
§Principal Scientist; strelets@mail.rcom.ru.

polar angle in the aft quadrant are very different, resulting in major differences in the polar directivities of the overall sound pressure levels at different azimuthal angles; these differences become pronounced when the jet velocity is increased. Significant noise reduction is achieved in the azimuthal directions below the longer lip of the beveled nozzle, principally in the polar angular range of ∼110 to ∼140 deg (the polar angles are measured from the jet inlet axis, with the jet exhaust corresponding to 180 deg). Furthermore, this reduction is observed at all frequencies. The magnitude of the noise reduction is a strong function of the jet velocity, with progressively higher reductions as the jet velocity is increased. In [14,15], the beveled nozzle is adapted for exhaust geometries typical of the high-bypass-ratio turbofan engines that power modern commercial aircraft. Specifically, the extended primary nozzle of a dual-stream nozzle configuration is beveled to achieve noise reduction. Just as for the single jet, the higher bevel angle of 45 deg (bevel45) was shown to yield larger noise benefits for the dual-stream jet, when static. However, the lower bevel angle of 24 deg (bevel24) was found to produce larger benefit in the effective perceived noise level for the realistic exhaust geometry in the presence of a flight stream. It was also noted in [14] that the thrust degradation at cruise due to bevel24 was <0.2% relative to a conventional exhaust system, with a potential for further mitigation of the thrust impact with better designs. In a high-bypass-ratio turbofan engine with bypass ratio greater than five, more than 75% of the thrust is produced by the fan stream. The typical plume deflection angle is ∼1.5 to ∼2.0 deg for the bevel24. This is why there is only a slight degradation of the thrust coefficient for the beveled nozzles; see Sec. 3 in [14] for a detailed discussion of the thrust performance of beveled nozzles.

Detailed analyses of the aeroacoustic measurements from single jets in [13] indicated that the noise reduction is due to the modification of the noise generated by the large-scale turbulence structures. For dual-stream jets, the noise generated by the large-scale structures in the inner shear layer was modified to obtain noise reduction. Recall that there is no explicit accounting for these structures in a Reynolds-averaged Navier–Stokes (RANS) simulation. Methods based on a two-step approach, but one in which the flowfield from a steady-state RANS computation is used as input to a synthetic noise model for use within the acoustic analogy, have so far failed to predict the change in spectral shapes with increasing polar angle, and therefore would be expected to fail to capture bevel effects. LES is ideally suited to investigate the noise mechanisms of beveled nozzles, because the principle behind this concept is based on the alteration of the noise radiated by the large-scale turbulence structures. Note that only two beveled nozzles (24 and 45) were tested. The current numerical simulations serve to provide detailed information on the entire flowfield which could perhaps lead to an optimization of the bevel angle. The objectives for considering this geometry are twofold: 1) get a better understanding of the underlying physical mechanisms that would potentially lead to the optimization of this concept for practical applications, and 2) test and validate the computational fluid dynamics (CFD)/computational aeroacoustics (CAA) approaches in a broader sense than in the core papers, as this geometry is simple enough but with a substantially different noise field from that of a round nozzle, thereby serving as an ideal candidate geometry for this purpose.

II. Overview of the Numerical Simulations

A. Characteristics of Jets Issuing from Beveled Nozzles

Figure 1 shows an isometric view of the dual-stream nozzle and the convention for the measurement of the bevel angle and the azimuthal angle. The azimuthal angles ϕ are measured as follows: 0 deg corresponds to the longer lip direction and 180 deg to the shorter lip in the orientation shown. D_1 is the diameter at the exit

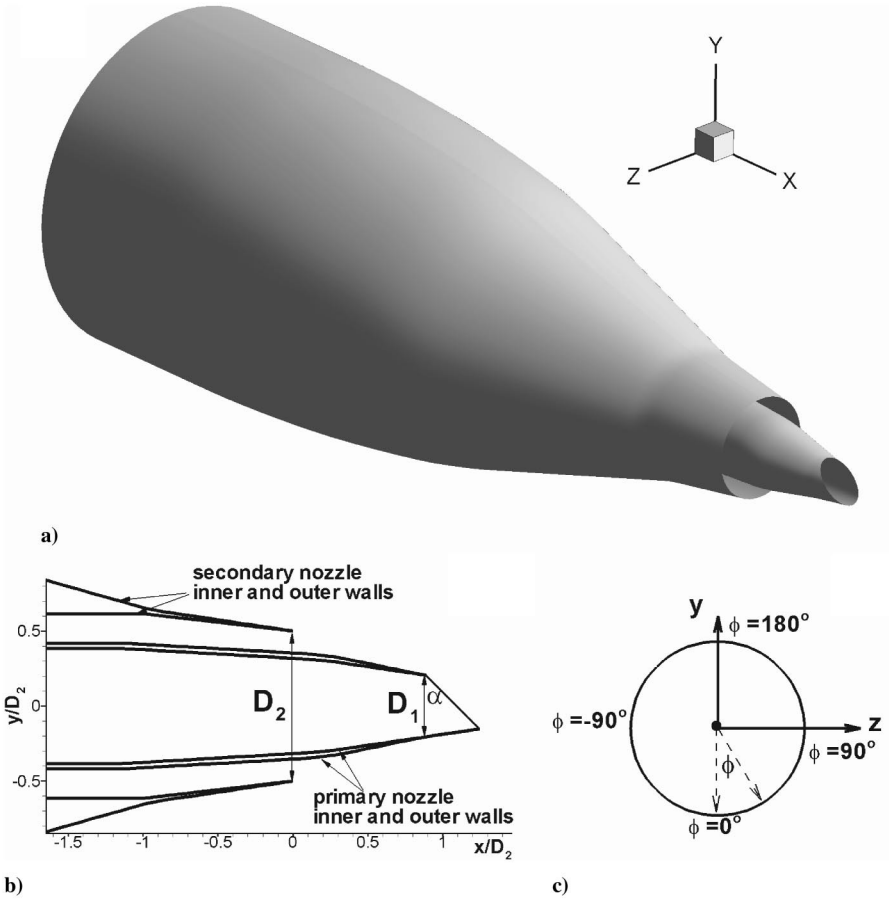

Fig. 1 Dual-staggered nozzle with beveled primary: a) isometric view, b) near-exit geometry, c) definitions of the bevel angle α and the azimuthal angle ϕ.

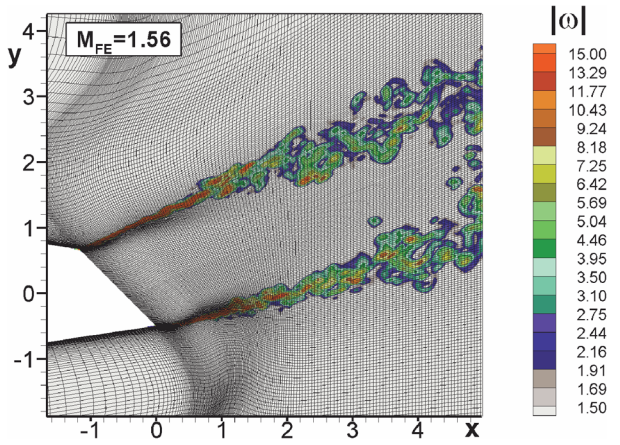

Fig. 2 Typical LES grid with ∼3.6 million grid points for the beveled nozzle, with snapshot of the vorticity field. $M = 1.56$, $Tt/Ta = 3.2$. Note that the grid clustering follows the development of the shear layer.

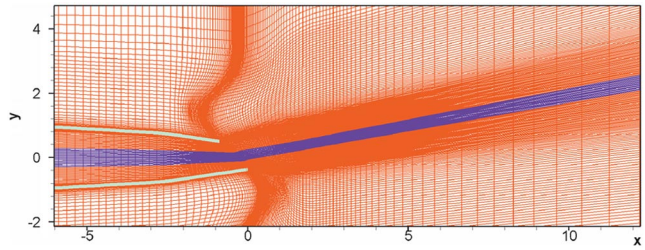

Fig. 3 Portion of the RANS grid (∼2.2 million points) in the flow symmetry plane used for single bevel45 nozzle.

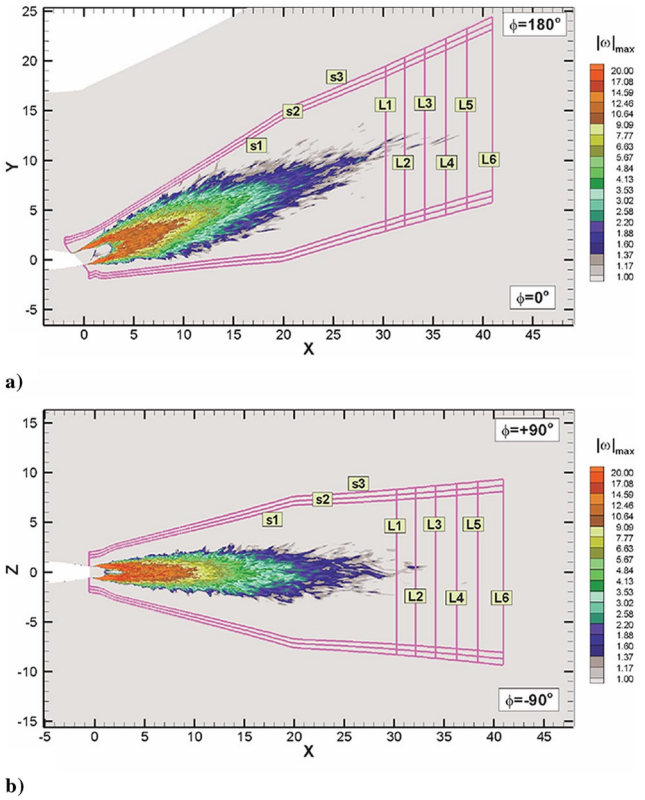

Fig. 5 Typical nested Ffowcs-Williams/Hawkings surfaces for noise computation. Surfaces in the symmetry plane (top) follow the vectored plume: a) side view, b) top view.

plane that corresponds to the short lip of the beveled nozzle; D_2 is the diameter of the round secondary nozzle. The beveled nozzle geometry requires special treatment in the simulations for the following reason: there is vectoring of the jet plume due to the beveled trailing edge, and the distribution of the flow parameters in the inclined exit plane is nonuniform. An examination of the nozzle geometry shown in Fig. 2 indicates that the flow exits the nozzle and encounters ambient pressure at the top (shorter lip of the beveled nozzle), while the flow is still accelerating at the bottom inside the nozzle at the same vertical axial location, closer to the longer lip. Therefore, the pressure distribution at the inclined nozzle-exit plane is nonuniform, with strong gradients top to bottom in the orientation shown. These types of flow features, where the flow parameters are not uniform and there could be vectoring of the jet plume, preclude the manual specification of inflow conditions. Therefore, the nozzle geometry and the flow inside the nozzle must be taken into account in the computations. This requirement necessarily increases the complexity and the needed computational power.

B. Prediction Methodology

As already mentioned, in this study, the numerical system developed in [1–3] is used for the investigation of the aeroacoustics of beveled nozzles. Therefore, only a brief overview of the prediction procedure is needed here. A high-order computer code, described by Strelets [16], is run on structured multiblock curvilinear grids. The versatility and the robustness of the code were demonstrated for a variety of aerodynamic flows and excellent comparisons with benchmark experimental data were shown in [16]. For jet noise predictions, the turbulence is treated by LES and the far-field noise is computed with the Ffowcs-Williams/Hawkings (FWH) [17] formulation. The Navier–Stokes equations are solved with a slightly upwind-biased high-order differencing for spatial discretization and implicit time integration. The time integration is carried out with a second-order three-layer backward scheme and dual time stepping. In the turbulent flow region and in the near field, the spatial discretization uses a combination of fourth-order centered and fifth-ordered upwind-biased schemes, based on flux-difference splitting

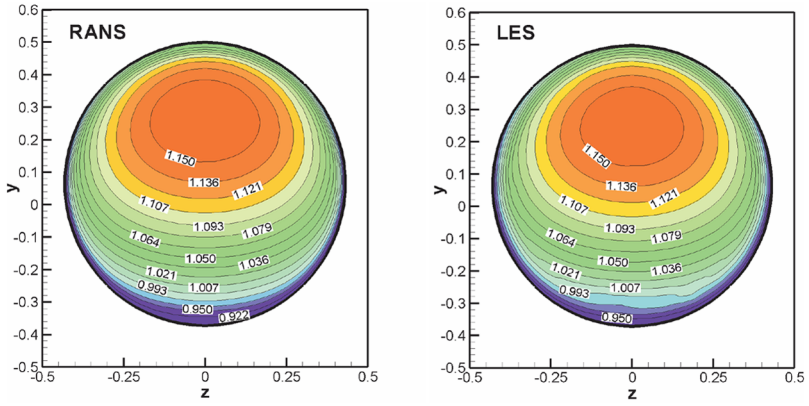

Fig. 4 Mean pressure p/p_a at the nozzle-exit plane (front view) obtained from RANS and LES. Single bevel45 nozzle; NPR$p = 1.89$, $Tp/Ta = 3.2$.

Table 1 Summary of the nozzle geometries and test conditions

Case no.	Core nozzle	Fan nozzle	NPRp	$(M_{\mathrm{FE}})p$	Tp/Ta	NPRs	$(M_{\mathrm{FE}})s$	Ts/Ta	M_f
1	round	——	1.28	0.6	3.2	——	——	——	0
2	round	——	1.89	1.0	3.2	——	——	——	0
3	round	——	4.00	1.56	3.2	——	——	——	0
4	bevel45	——	1.28	0.6	3.2	——	——	——	0
5	bevel45	——	1.89	1.0	3.2	——	——	——	0
6	bevel45	——	4.00	1.56	3.2	——	——	——	0
7	round	round	1.8	0.96	2.37	1.8	0.96	1.0	0
8	bevel24	round	1.8	0.96	2.37	1.8	0.96	1.0	0
9	bevel45	round	1.8	0.96	2.37	1.8	0.96	1.0	0
10	round	round	1.8	0.96	2.37	1.8	0.96	1.0	0.2
11	bevel24	round	1.8	0.96	2.37	1.8	0.96	1.0	0.2
12	bevel45	round	1.8	0.96	2.37	1.8	0.96	1.0	0.2

for the inviscid terms. Outside this region, purely upwind differencing is employed to damp out the outgoing waves. A buffer layer, in addition to nonreflecting boundary conditions, is included to ensure that reflections from the boundaries do not contaminate the solution in the domain of interest. For simulating the turbulence, the subgrid-scale (SGS) model is deactivated, and the approach is viewed as "implicit LES." The slight dissipation introduced by the upwind scheme (with a typical weight of 0.25) serves the purpose of removing the energy that would be transferred to the unresolved scales as part of the energy cascade. Several other approaches were evaluated as well; this choice turned out to be the best option for simulating realistic transition to turbulence, as explained in [1–3].

As previously stated, the internal flow has to be computed for the beveled nozzle to provide the flow conditions at the nozzle exit. However, most of the radiated noise is generated in the external plume for the simple geometries considered here; complex nozzles such as internal lobed mixers might require a different treatment. There are two options for treating this problem. The first option, that of large-eddy simulation of the entire flowfield, internal and external, is beyond the computational resources available to us, and perhaps is not necessary for noise predictions because the noise is generated external to the nozzle. At practical Reynolds numbers, the computer requirements would become prohibitive even for mainframe computers; a key contributor to the cost is the resolution of the viscous sublayers inside the boundary layers. Therefore, a two-step approach has been adopted. A steady RANS simulation is first carried out for the internal and external plume that ensures an accurate resolution of the nozzle boundary layer; an example of the RANS grid is presented in Fig. 3. The typical value of the near-wall grid step in the computations is $10^{-4}D_1$, which results in the values of the near-wall step in the log-law coordinates in the range of 0.5–2.5 (the maximum values occur only in the close vicinity of the nozzle exit near the lower wall of beveled nozzles). The number of node points in the nozzle boundary layers is about 30. Note that a grid refinement performed for several cases has shown that the RANS solutions are grid-independent, at least in the area close to the nozzle

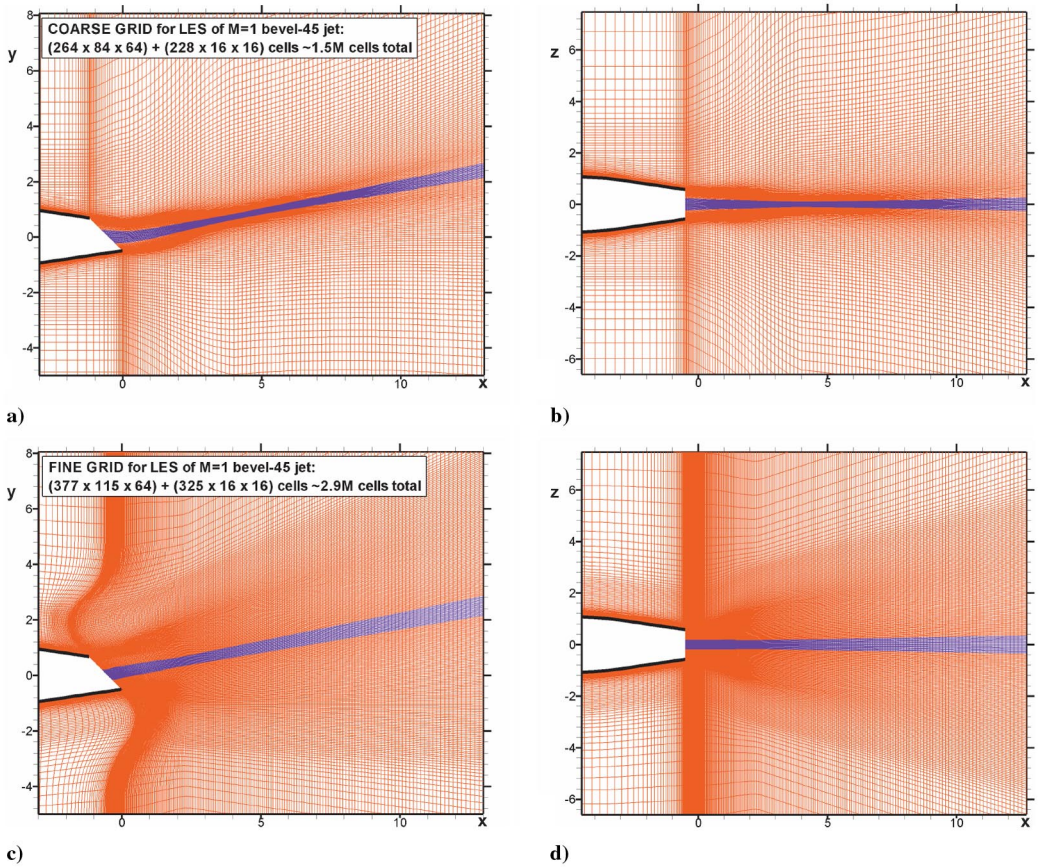

Fig. 6 Portions of the coarse and fine LES computational grids in the *XY* and *XZ* planes for the bevel45 nozzle.

exit, which is the only area of the RANS solutions used in the subsequent LES of the jet plume.

The computations are performed with the use of the ν_t-92 model, which is a one-equation linear isotropic eddy-viscosity transport model developed since the 1970s by Secundov (see [18,19]), and is more attractive than other common models for round jets because of a correction term activated by the curvature of the eddy-viscosity contours (however, this applies to the fully developed jet region, not to the thin mixing layers which separate the potential cores). It also contains a compressibility correction, which is felt in sonic mixing layers. We note that the complexity in the present flows is primarily inviscid in nature: transverse pressure gradients and compressibility on the potential core. The boundary layers remain thin and attached thanks to the contraction, so that the impact of turbulence-modeling imperfections is slight.

An LES is performed in a second step for the external plume on a coarser grid in the radial direction near the nozzle wall edge (resolving the viscous sublayer not being necessary), with the total pressure and temperature and the inflow velocity angles from the RANS simulation interpolated and specified as the inlet boundary condition. The inlet pressure for the subsonic jets is calculated from a standard nonreflecting boundary condition. Figure 4 shows a comparison of the mean pressure fields at the nozzle-exit plane obtained from RANS and LES. It has been verified that the time-averaged static pressure field from the LES matches that from the coupled RANS simulation everywhere except for a very thin near-wall region, thus validating the two-step approach. The LES grids are, on the other hand, finer and more uniform in the streamwise direction, which is essential for simulations aimed at noise predictions. They have from ~1.5 to ~4.5 million nodes, depending on the geometry and cycle conditions (a fragment of a typical fine grid used in the LES stage of the two-stage procedure is shown in Fig. 2 together with the vorticity contours). The computational domain extends typically to $75D$ in the axial direction; in the radial direction, the grid extends to $10–15D$ upstream of the nozzle exit and progressively widens in the axial direction to accommodate the spreading jet, so that the half-width of the domain reaches up to $\sim 40D$ at the last axial station (here, $D = D_1$ for the single nozzles and $D = D_2$ for the dual-stream geometries).

There is now much work on hybrid RANS–LES approaches, which has revealed some weaknesses, in particular when a wall-bounded shear flow involves the exchange of unsteady content between a RANS layer very close to the wall, and an LES layer along it. The exchange here is of a different nature, as the information flowing from RANS to LES consists in steady velocity profiles, in which the most important quantity is the exact direction of the velocity vector. The RANS solution also provides the nozzle-exit boundary-layer thickness, but no unsteady content; this would require vastly finer grids than are affordable. Given a steady but thin inflow boundary-layer profile, the LES achieves transition in the mixing layer without any artificial forcing like it did in [1,2] with analytical velocity profiles.

In a recent upgrade to the numerics, the ability to handle supersonic jets with shocks in the jet plume was improved, as described in [3]. A zonal method had been adopted in [1,2], where the order of the finite differencing was lowered from a fifth-order to a third-order scheme for the upwind differencing, and a flux-limiter was activated in the regions where shocks were expected to form and assumed to be known a priori. This approach is not entirely satisfactory, because it is not possible to know where the shocks would be located for flows from complex geometries. A method for local automatic activation of the flux-limiters was developed and tested for several jet Mach numbers from round and beveled nozzles by Shur et al. [3]; the adopted algorithm was robust and more accurate than the zonal method.

The far-field noise is calculated through surface integrals, using the permeable FWH formulation. The FWH surface has a funnel shape and a closing disc at the downstream end; because turbulence crosses this disk, the accuracy depends on a change of variables from density to pressure in the FWH equation, especially with hot jets [20]. The design of the funnel is the same as for simpler jets: namely, the innermost sleeve is slightly out of reach of any turbulent fluid, and results from somewhat looser sleeves are used for comparison. The natural design of the grid allows the funnels to coincide with grid surfaces, as before. The observer points are located on a polar arc of 20 ft (6.91 m), with the origin of the coordinate system located on the jet axis at the nozzle-exit plane of the primary nozzle.

Computations on multiblock structured grids are performed on personal computer clusters. Therefore, the number of grid points is lower than on mainframe machines. However, the resolved frequency range is not dramatically narrower, because of the chosen grid topology, the efficient distribution of the grid points, and the tight FWH sleeve which minimizes the amount of numerical dissipation. The highest resolved Strouhal number for the single jets considered below varies from ~1.5 to ~3 depending on the test case and the number of grid points; for dual jets, it is ~8 based on fan-nozzle diameter and fan velocity. Noise predictions from a variety of geometries and flow conditions such as single and dual-stream jets, jets with coflow, chevron nozzles, etc., have already been carried out and presented in [1–3].

For the stringent case of the beveled nozzle, issues of grid clustering in LES, shape and location of the FWH surface, etc., had to be addressed afresh. To accommodate the plume deflection from the beveled nozzles, the FWH surfaces, like the grid, are turned toward the shorter side of the nozzle. Figure 5 shows typical FWH surfaces

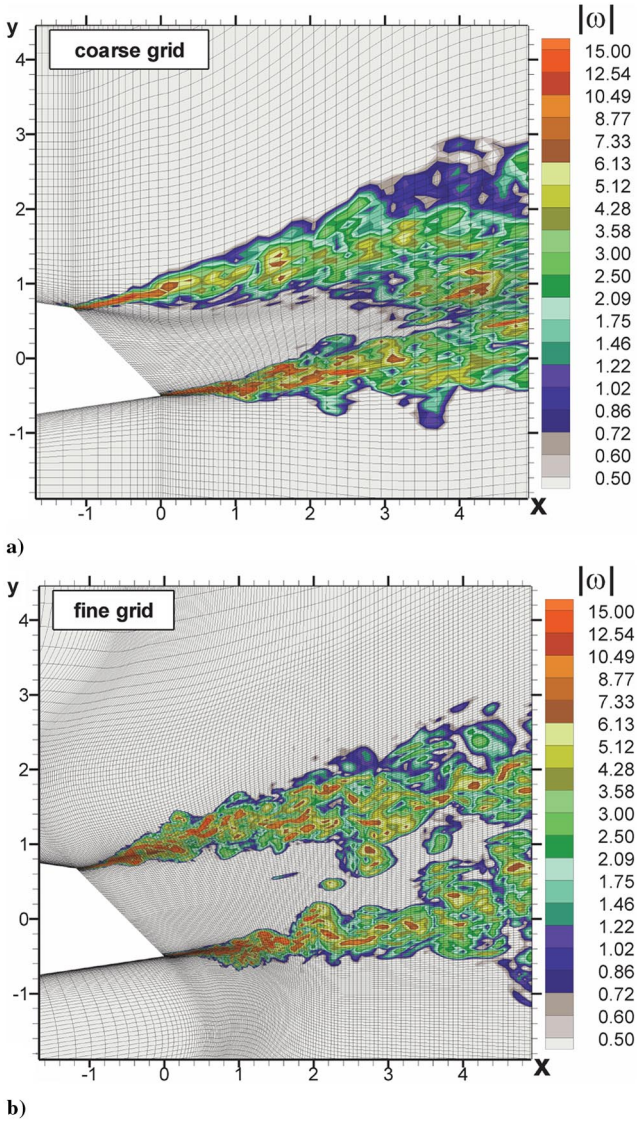

Fig. 7 Details of the grid in the *XY* plane and vorticity snapshots in the near-nozzle region. Bevel45 nozzle, $M = 1.0$, $Tt/Ta = 3.2$.

for the beveled nozzle, in both side and top views. The side view or vertical jet symmetry plane (Fig. 5a) is termed the *XY* plane; the top view (Fig. 5b) is the projection of the grid surface normal to the symmetry plane *XY* and slanted to track the jet plume on the horizontal plane *XZ*. Hereafter, such a view or horizontal plane is termed the *XZ* plane in the plots. Also shown in this figure are the contours of maximum vorticity magnitude. It is clear that the highest levels of vorticity are concentrated in the shear layers and in the region downstream of the end of the potential core. Several issues on the placement of the FWH surfaces, the use of the closing discs at the downstream end, the need to average over several closing discs, etc., have been addressed in detail in [1,2].

III. Results and Discussion

A. Comparison of Flow Parameters with Experiments

Table 1 provides a summary of the various test cases, both for single and dual-stream nozzles, which have been considered in this paper. The nozzle pressure ratios (NPR) and the stagnation temperature ratios are listed, along with the jet Mach number (fully

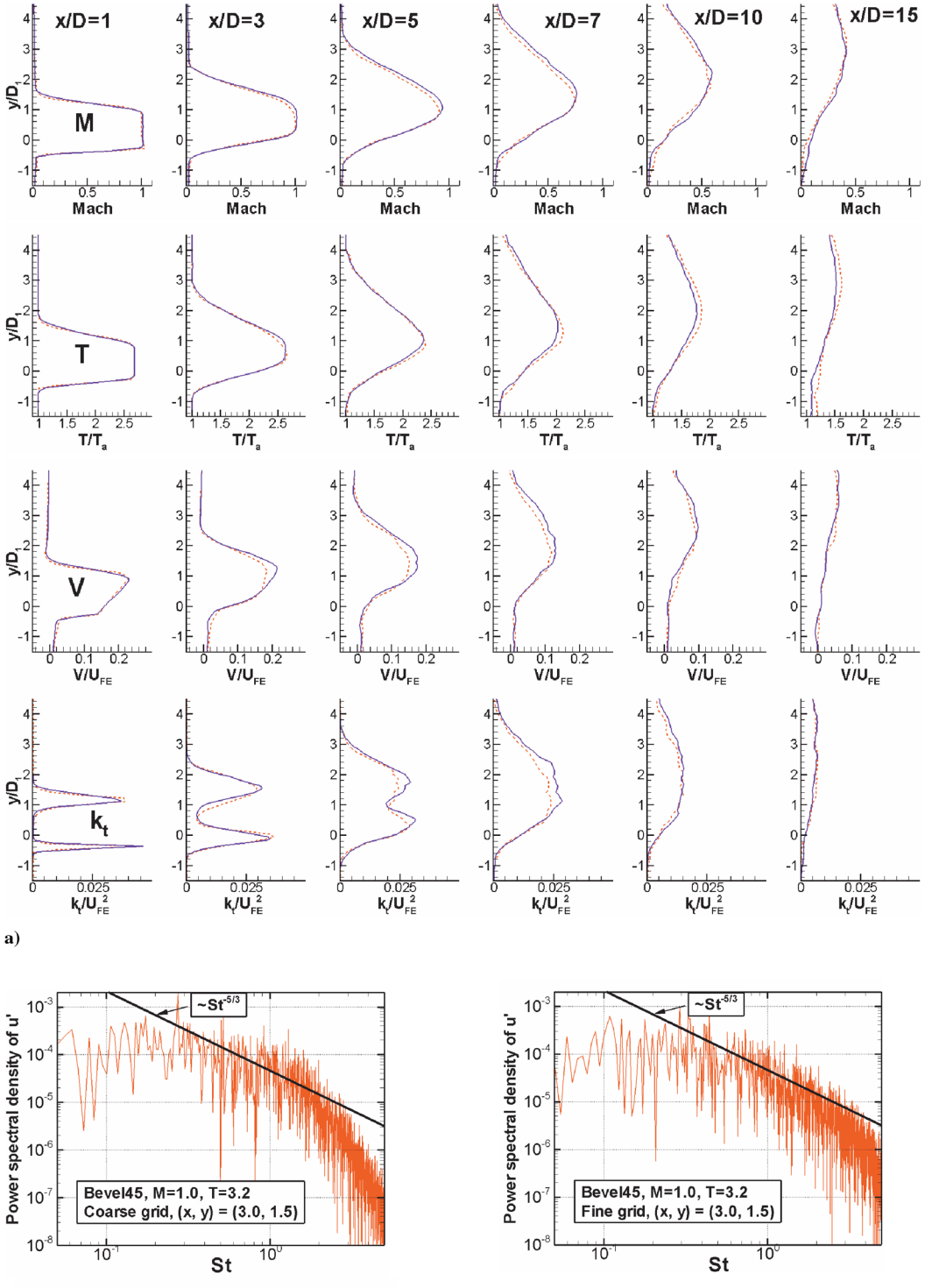

Fig. 8 a) Effect of grid on the distribution of time-averaged parameters in jet's symmetry plane. Bevel45 nozzle, $M = 1.0$, $Tt/Ta = 3.2$. Dashed lines: coarse grid; solid lines: fine grid. First row: Mach number; second row: temperature (normalized with ambient temperature); third row: vertical velocity (normalized with the fully expanded jet velocity U_{FE}); fourth row: turbulent kinetic energy. b) Spectra of streamwise turbulence intensity from LES on the coarse and fine grids.

expanded for the supersonic cases) and the flight Mach number M_f. The subscripts p and s denote the primary and secondary streams, respectively.

First, the accuracy of the RANS calculations for the nozzle internal flow is verified with the experimental measurements of [13]. The performance of two different beveled nozzles, with bevel angles of 45 deg (bevel45) and 24 deg (bevel24) (see Fig. 1) were evaluated in the experiments. The measurements indicated that because of the nonuniform pressure distribution for the beveled nozzle at the nozzle-exit plane, the effective nozzle flow area is less than the geometric area. Consequently, there is a reduction in the nozzle discharge coefficient. The measured nozzle discharge coefficient is $\sim$13% less for bevel45 compared with the round nozzle, and the difference is 13.6% from CFD. Note that the round nozzle extends to the edge of the shorter lip of the beveled nozzle. All the distances are nondimensionalized by the following characteristic lengths: the primary jet diameter for the single jets and the fan diameter for the dual-stream jets. This close agreement is attributable to the fact that the effect is mainly inviscid. The computed plume deflection angle for a Mach number $M = 1.0$ jet is 11 deg, whereas it is $\sim$10 deg in the measurements. Thus, the predicted integral quantities are in good agreement with measurements. For bevel33, the discharge coefficient in the computations is 0.895 and the deflection angle is 8.5 deg. Though no measurements are available at this bevel angle, it is noted that these values for bevel24 are 0.92 and 7 deg, respectively. Thus, the effect of the bevel angle on nozzle discharge and thrust coefficients for the round and beveled nozzles are accurately captured by the RANS simulations, thereby giving us confidence that the correct inflow conditions are prescribed for the LES of the external flow.

There are no mean-flow or turbulence measurements for the beveled nozzle. However, the accuracy of LES for the external plume has been assessed for a round jet recently in [21]. The predicted time-averaged centerline variations from the LES have been compared with measured data. The distributions of the axial velocity and the

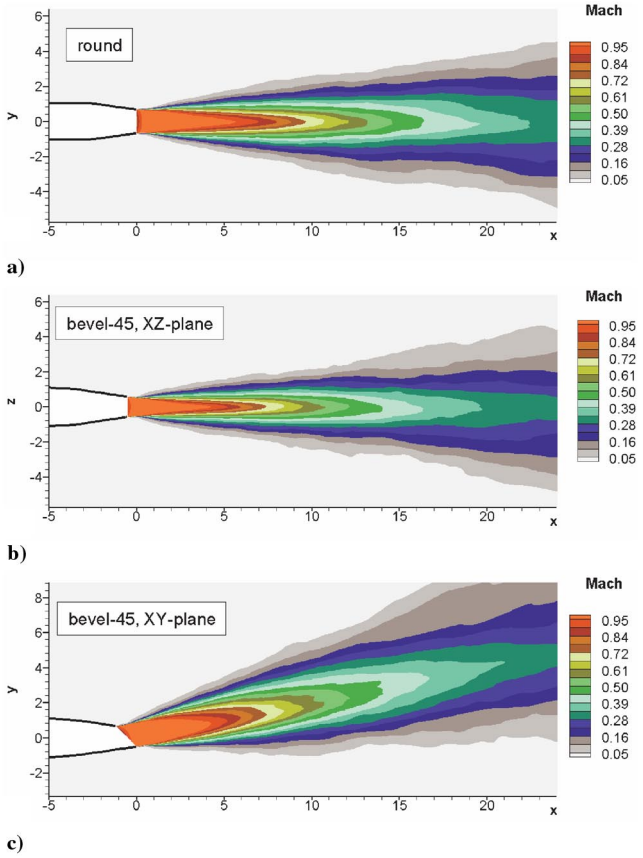

Fig. 10 Comparisons of the Mach number contours between round and bevel45 nozzles. $M = 1.0$, $Tt/Ta = 3.2$.

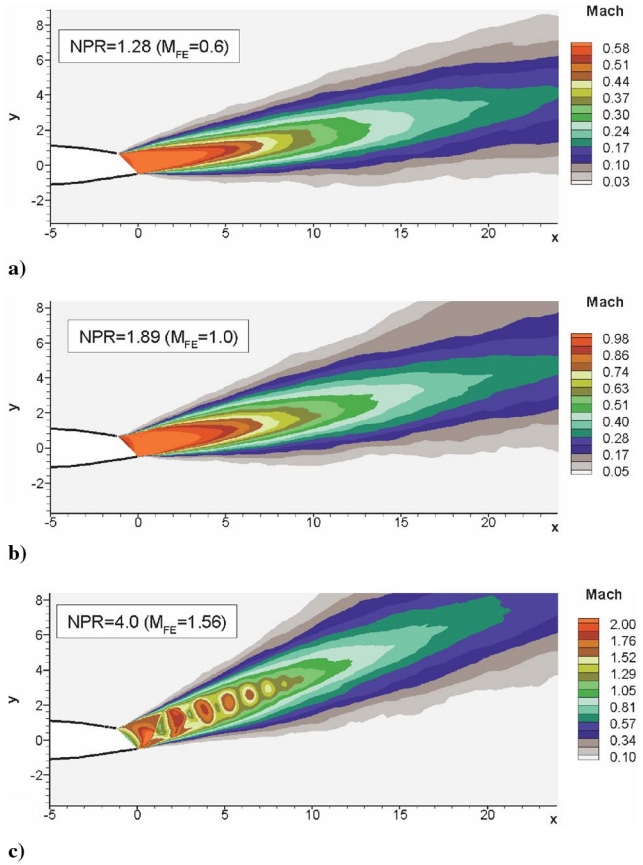

Fig. 9 Distribution of Mach number in the XY plane for bevel45. $Tt/Ta = 3.2$.

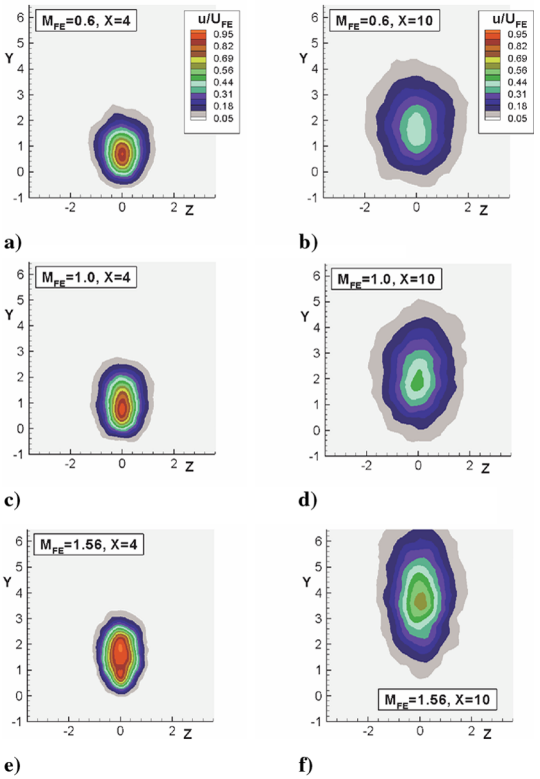

Fig. 11 Effect of Mach number on the streamwise velocity distribution in two cross-sectional planes for the bevel45. Time-averaged LES results. $Tt/Ta = 3.2$.

root-mean-square values of the axial and radial velocity fluctuations are in very good agreement with experimental data; see Fig. 10 in [21]. It is assumed here that the results of the LES of the external plume for the beveled nozzles are also quite accurate, because the same practices in grid design and numerics are followed in all simulations.

B. Grid Design and Distribution

The vectoring of the jet plume introduces additional considerations for the design of the computational grid and the clustering of the grid points in the shear layers. There is no a priori knowledge of the angle of the plume deflection for a given bevel angle; therefore, during the first stage of the simulation (RANS), a trial and error approach with different grids is attempted. This knowledge is then used when building the grid for the LES of the plume, and the grid is adapted to the real positions of the shear layers. Apart from the critical need for the proper positioning of the grid for the beveled nozzle, a grid-refinement study was carried out for both the round and bevel45 nozzles. The results from this exercise for the round nozzle are reported in Sec. IV.A in [21]; the main findings are summarized here for completeness.

First, a brief explanation is in order, because the grid refinement for noise prediction is slightly different than it is for the resolution of the flow. A detailed knowledge of the important regions of noise production in single as well as dual-stream jets is vital to achieve good spectral predictions. There are two main source regions for high-speed jets: one is located on the jet centerline beyond the end of the potential core, and is several jet diameters in spatial extent. This is the dominant source region for jets with subsonic convective velocities. There is an additional expanded source of noise, due to Mach wave emission, in the initial developing shear layer, starting close to the nozzle-exit plane for convectively supersonic jets.

The test case chosen was a heated jet with $M = 1.0$ and a stagnation temperature ratio Tt/Ta of 3.2, which has both the sources of noise. Figure 6 shows a portion of the coarse and fine grids close to the nozzle. The coarser grid had a total number of grid points of $\sim$1.5 million for LES; the finer grid had $\sim$2.9 million grid points. To target the two sources, the fine grids were significantly denser (by more than a factor of two) in the axial direction, in the regions of importance for noise. Additionally, the region with the fine grid was extended outward in the radial direction, enough to reach the FWH surface. The time step was reduced from 0.03 to 0.02, normalized with diameter and jet velocity; on the other hand, the azimuthal grid spacing was unchanged. This radial refinement had a most beneficial effect in that the resolved frequency (Strouhal number) range was extended considerably. In other words, the grid was refined not only in the simple sense of having more points, but also in terms of a more educated design.

Figure 7 shows snapshots of vorticity obtained with the two grids. There is much better resolution of the developing shear layers with the finer grid, as the region of the grid clustering in the radial direction is adjusted to the position of the jet shear layers. The time-averaged distributions of several parameters (the Mach number, the static temperature, the vertical velocity, and the turbulent kinetic energy) on the symmetry plane are shown in Fig. 8a at nondimensional axial locations of 1, 3, 5, 7, 10, and 15. The differences between the two sets of solutions are not striking. Figure 8b depicts the effect of the grid refinement on the shear layer turbulence. It reveals a sufficient drain of energy to the unresolved scales on both grids and an extended inertial range in the spectrum from the fine-grid simulation, which supports the credibility of the LES even with the deactivated SGS model. For the shock-containing supersonic jet, with $M = 1.56$ and $Tt/Ta = 3.2$, the grid had to be refined to capture the shock position, and so the number of grid points was increased to $\sim$3.6 million (a close-up of the grid and the vorticity distribution for this supersonic case is shown in Fig. 2).

An important finding from [21] related to the grid refinement was that the effect of the grid refinement on the centerline distributions of axial velocity, temperature, and the root-mean-square value of the axial fluctuation velocity were minor (the results shown here for the beveled nozzle are consistent with the finding for the round nozzle). However, there was a dramatic improvement in the noise predictions with the finer grids. The range of resolved Strouhal numbers was almost doubled, providing better agreement with measured spectra. Further, the predicted peak radiation angle was shifted aft by

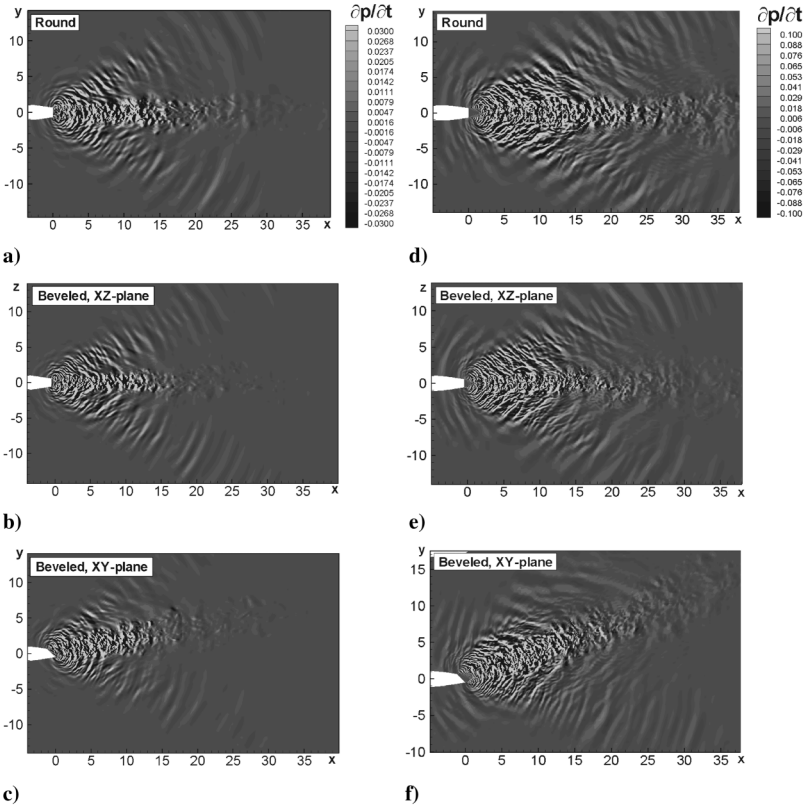

Fig. 12 Snapshot of pressure-time derivative for round and bevel45 in the *XY* and *XZ* planes. $Tt/Ta = 3.2$. a–c): $M = 1.0$, d–f): $M = 1.56$.

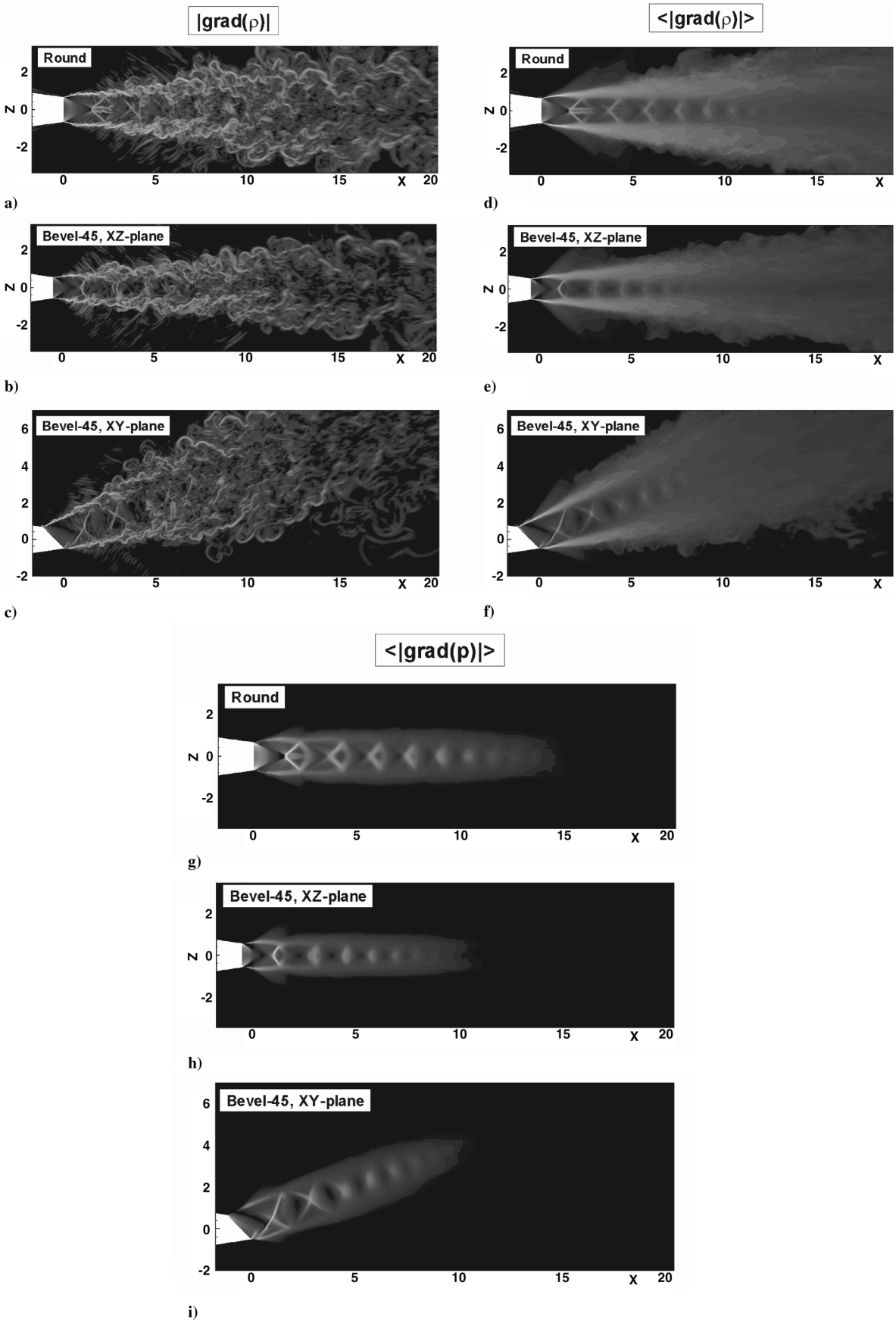

Fig. 13 Numerical schlieren for the round nozzle and bevel45. $M = 1.56$, $Tt/Ta = 3.2$. a–c): instantaneous density gradient, d–f) time-averaged density gradient, g–i) time-averaged pressure gradient.

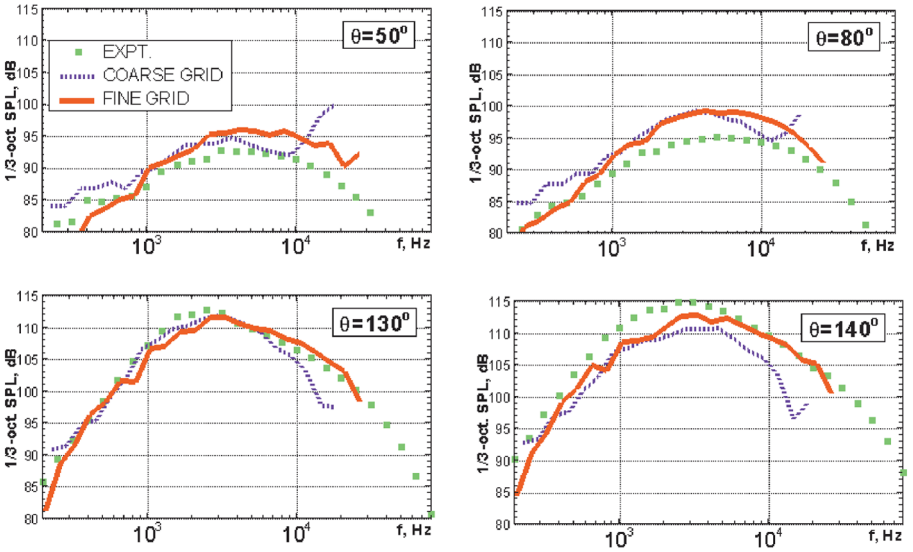

Fig. 14 Comparisons of spectra obtained using coarse and fine grids with data. Round nozzle, $M = 1.0$, $Tt/Ta = 3.2$.

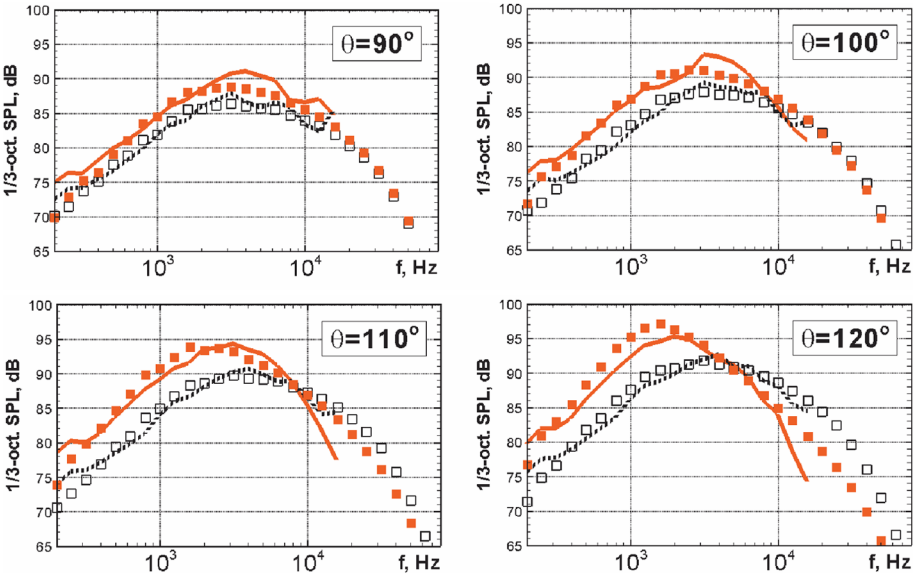

Fig. 15 Comparison of predicted spectra with data. Bevel45, $M = 0.6$, $Tt/Ta = 3.2$; solid lines, filled square: 180 deg azimuthal angle; dashed lines, open squares: 0 deg azimuthal angle (below longer lip).

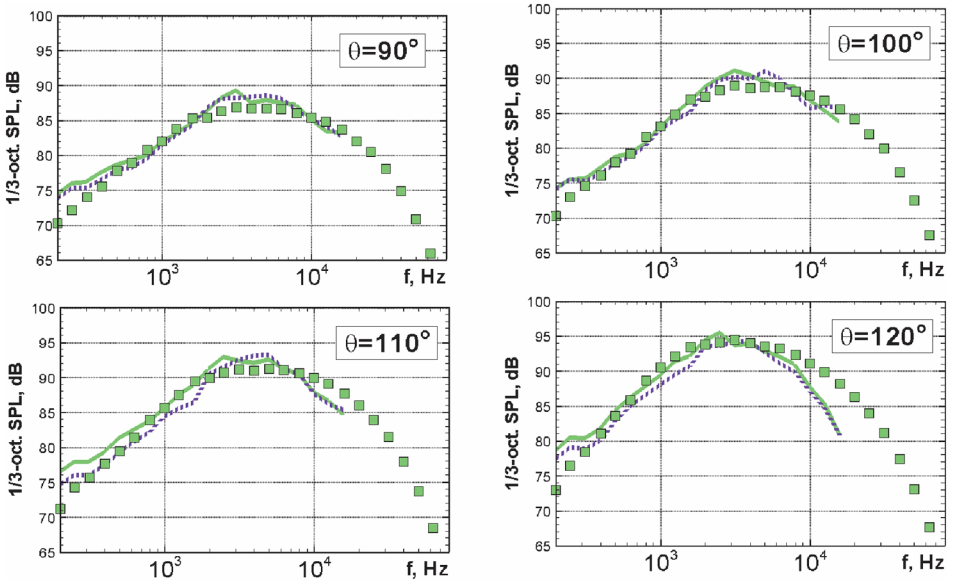

Fig. 16 Comparison of predicted spectra with data. Bevel45, $M = 0.6$, $Tt/Ta = 3.2$.

~5 deg, improving agreement with data. It was concluded in [21] that it is important to resolve the subtleties of the flow features responsible for noise generation and radiation. Thus, it should be clear that extreme care has to be exercised in the design of the grid for obtaining good noise predictions.

The nondimensional time step in the LES of the cases listed in Table 1 varied from 0.012 for the dual-stream jets (cases 7–12) and the supersonic underexpanded jets (cases 3, 6) to 0.03 (cases 1 and 4, computed only on the coarse grids of ~1.5 million points). With these time steps, the Courant–Friedrichs–Lewy (CFL) number (defined by the minimum streamwise grid step and by the velocity of the primary jet) in all the simulations is less than 1.2. To let the transients convect out of the computational domain, the simulation is run for 500–800 convective time units D/U_{jet} for the static jets and 300–400 time units for jets in a flight stream. The sampling for time-averaging and storing of the information for the noise postprocessing is started after this transient period and is typically performed over 200 time units. This is the same procedure adopted in [1]. The time histories of the necessary variables on the FWH surfaces are saved, only every sixth time step and not at every time step of the simulation. This practice is sufficient to address the frequency range represented by the LES. The CPU time on a six-processor PC cluster with Pentium 4 3000 kHz processors varied from 10 days to 2 months depending on the grid used.

C. Single Jets

The beveled nozzles exhibit several interesting noise characteristics, as already noted. The predicted aerodynamic performance of the beveled nozzles was shown to agree with the measurements in Sec. III.A. For the simulations, the highest temperature ratio of 3.2 has been considered from a vast database to increase the jet velocity for a given Mach number and thereby accentuate the differences in the noise characteristics. Simulations have been carried out at three different Mach numbers of 0.6, 1.0, and 1.56; the shock-containing supersonic jet represents a stringent test case for testing the numerics. Results from the round nozzle are also included in some figures, so as to highlight the differences in the flowfield and noise between the two geometries. The time-averaged Mach number contours in the XY plane from the LES stage of the two-stage RANS–LES technique for

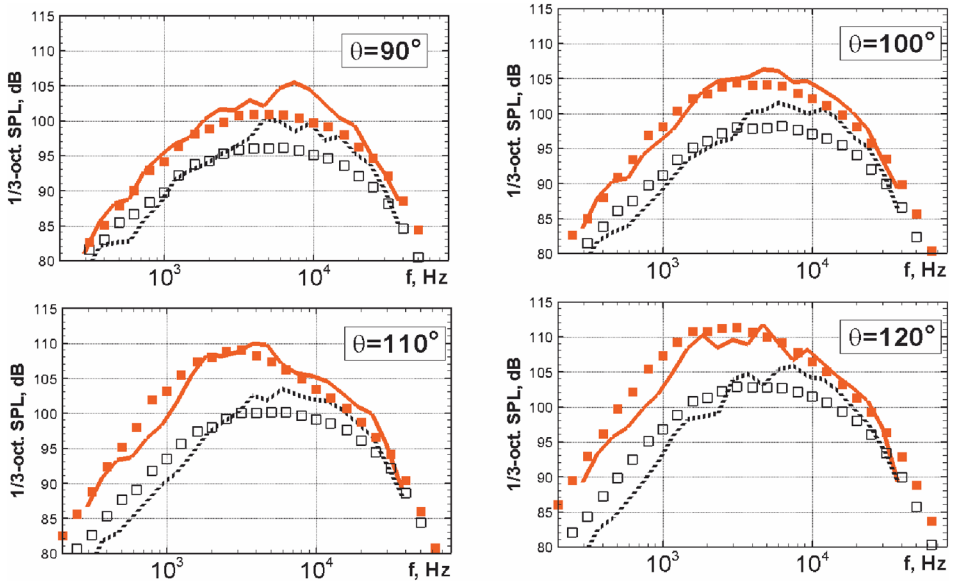

Fig. 17 Comparison of predicted spectra with data. Bevel45, $M = 1.0$, $Tt/Ta = 3.2$; solid line, filled square: 180 deg azimuthal angle; dashed line, open square: 0 deg azimuthal angle (below longer lip).

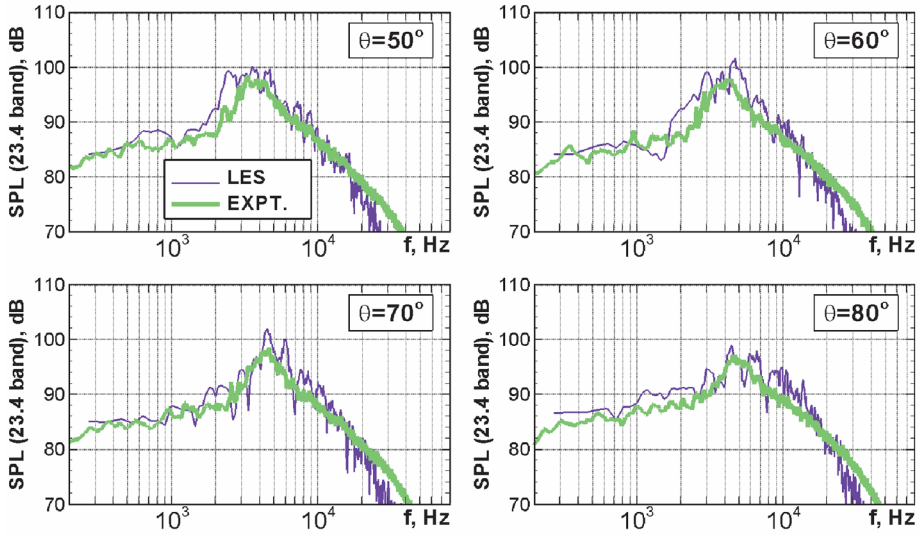

Fig. 18 Comparison of spectra with significant broadband shock-associated noise. Bevel45 nozzle, azimuthal angle = 0 deg. $M = 1.56$, $Tt/Ta = 3.2$; thin lines: prediction; thick lines: data.

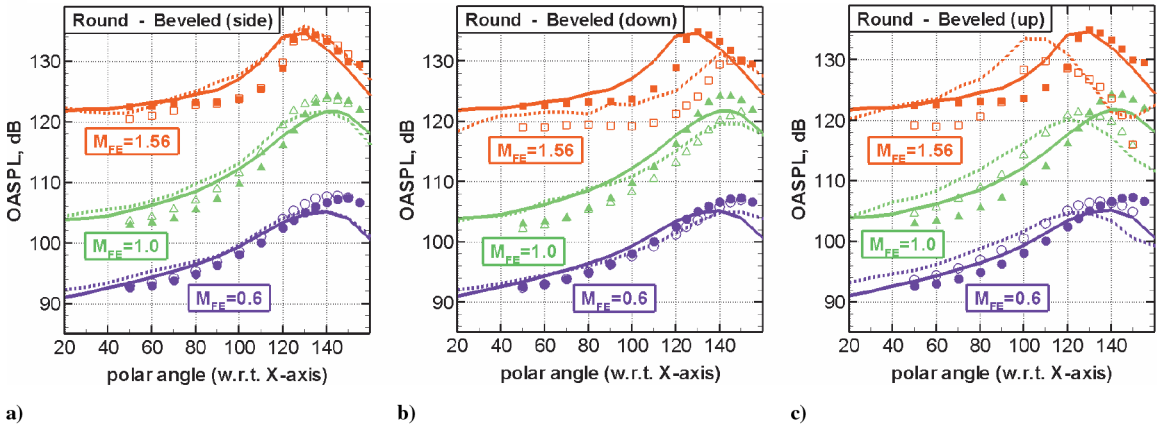

Fig. 19 Comparisons of OASPL directivities at various azimuthal angles. $Tt/Ta = 3.2, M = 0.6, 1.0, 1.56$. Filled symbols: round data; solid line: round LES; open symbols: bevel45 data; dashed line: bevel45 LES. a) azimuthal angle = 90 deg; b) azimuthal angle = 0 deg; c) azimuthal angle = 180 deg.

the three cases are shown in Fig. 9. The plume deflection angle is more pronounced for the supersonic jet. Figure 10 shows a comparison of the plume development in the two planes of the beveled nozzle with the corresponding one for the round nozzle, at a Mach number of 1.0. Analysis of these results indicates that the development of the two shear layers in the XZ plane is symmetric, whereas the plume deflection is evident in the XY plane. This figure and the cross-sectional cuts of the streamwise velocity shown in Fig. 11 illustrate that the widths of the jets are different in the two planes; the jets are squeezed in the XZ plane and are elongated in the XY plane, with the plume assuming an oval shape. This deformation of the jets is more pronounced for the higher bevel angle and for jets at higher Mach numbers. It is worth noting here that the flowfields computed with the RANS (not shown) and LES are qualitatively similar.

Next we examine the noise fields. Snapshots of the $(\partial p/\partial t)$ field are shown in Fig. 12 for two different Mach numbers of 1.0 and 1.56. This quantity is normalized by $(\rho_\infty a^3/D_1)$, the ambient values of density, the speed of sound, and the jet diameter. The different wave patterns are best seen in these plots; the Mach wave emissions for the round nozzle and for the bevel45 in the XZ plane are symmetric. In the XY plane for bevel45, the directional radiation is beamed to a lower polar angle for the shorter lip side. For the $M = 1.56$ jet, a Mach disc forms for the round jet; there is subsonic flow with an internal shear layer downstream of the Mach disc. This can be seen in the density gradient fields or "numerical schlierens" of the flow shown in Fig. 13. The instantaneous density gradient field is presented in Figs. 13a–13c. The time-averaged density field shown in Figs. 13d–13f includes the temperature effect and produces a "smeared" image of the flow; this is not the case with the pressure field as the temperature effects are decoupled. Therefore, the time-averaged field of the pressure gradient provides a clearer picture for hot jets, as depicted in Figs. 13g–13i. A system of shock cells interacting with turbulence is noticeable for both nozzle geometries. For the bevel45, there is no Mach disc and the shocks are damped out faster, with considerably fewer shock diamonds in the plume. As can be appreciated, there are distinct differences in the flowfield and the wave patterns associated with the beveled nozzles. Therefore, we should expect changes in the noise field as well.

The improvements in the predicted spectra with the grid refinement are illustrated with a single example for the $M = 1.0$ jet with $Tt/Ta = 3.2$. Comparisons of the predicted spectra from the coarse grid (~1.5 million points) and fine grid (~2.9 million points) with data are shown for the round nozzle in Fig. 14 at various polar angles of 50, 80, 130, and 140 deg. First of all, there is a drastic improvement in the predicted spectral shapes with the fine grid, and the highest resolved frequency reaches ~25 kHz. There is almost a doubling of the range of well-predicted Strouhal numbers, from ~1.35 to ~2.7; the predicted peak levels are also ~3 dB higher at the aft angles, thereby moving them closer to data (see [21] for more details). Note that the widening of the resolved frequency range with the grid refinement observed in the simulations agrees fairly well with an estimation of the maximum resolved Strouhal number. This high-frequency limit is calculated as an inverse radial grid step on the FWH surface, assuming that six cells per wave length are sufficient for an accurate sound resolution: $St_{\max} = aD_p/(6\Delta r U_p)$. This estimation is confirmed by the fact that the spectra start to exhibit unnatural behavior (tail-up or sharp drop) very close to that defined maximum value for the Strouhal number.

In Figs. 15 and 16, comparisons for bevel45 at Mach 0.6 with data at different azimuthal angles are presented. For this test case, only the coarse grid (~1.5 M nodes) results are available. The maximum resolved Strouhal number for this case is ~1.5, which corresponds to a model scale frequency of 8600 Hz. The tail-up at a frequency of

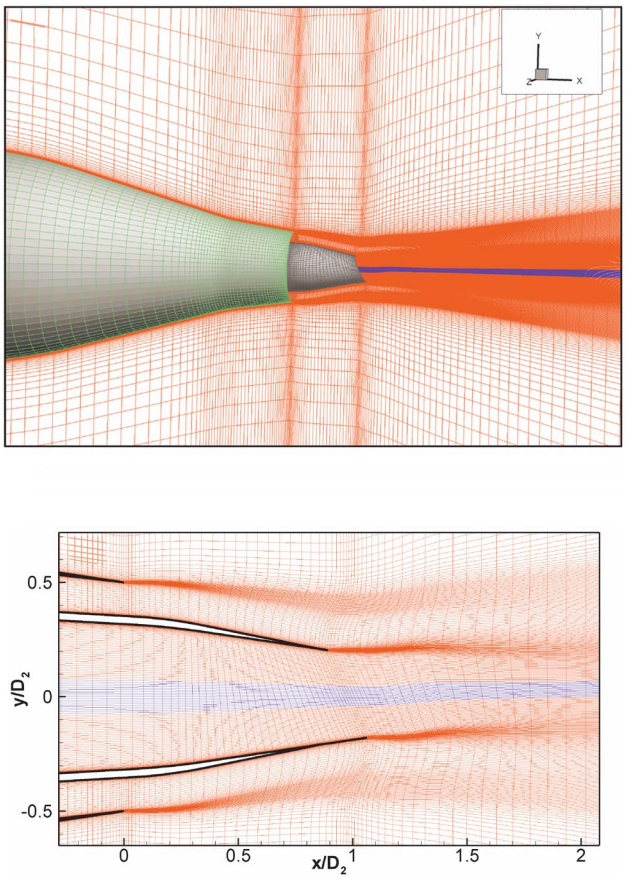

Fig. 20 Portion of the RANS grid used for dual-stream beveled nozzle. a) XY grid in the near-nozzle region and nozzle surface grid; b) close-up view of the resolution of the shear layers.

$\sim$11 kHz is due to numerics; note that this problem has since been eliminated (with a fine grid) in Fig. 14 for the $M = 1.0$ jet at the same temperature. The predicted trends are in good agreement with data for the two azimuthal angles of 0 and 180 deg in Fig. 15; there is a $\sim$3 to $\sim$5 dB increase in the low-frequency noise radiated to the shorter side of the bevel (180 deg), which is captured very well in the simulations. Viswanathan [13] carried out a detailed analysis of the variation of the spectral shapes at various polar and azimuthal angles, by comparing the measured shape against the analytical shapes extracted by Tam et al. [22]. Tam identified two distinct shapes termed the fine-scale similarity (FSS) shape dominant at the lower polar angles and the large-scale similarity (LSS) shape dominant in the peak radiation sector at large aft angles. It was noted in [13] that the spectral shapes at an azimuthal angle of 180 deg attains the LSS shape at lower polar angles, whereas the shapes retain the FSS shapes for the round nozzle, and the beveled nozzle at an azimuthal angle of 0 deg. See Sec. IV.C in [13] for a detailed discussion of the noise generation mechanisms of the beveled nozzles. It was also shown that at a polar angle of $\geq$ 110 deg, the LSS shape is observed for this particular case of $M = 0.6$ and $Tt/Ta = 3.2$; see Fig. 21 in [13]. The FSS shape is retained at two polar angles of 110 and 120 deg for the round nozzle (see Fig. 22 in [13]); that is, even if we account for the plume deflection of $\sim$10 deg for the beveled nozzle, there is a drastic change in spectral shape for the beveled nozzle. A closer examination of the spectra at 120 deg in Fig. 15 reveals that the predicted spectrum at an azimuthal angle of 180 deg indeed has the LSS shape, whereas the spectrum at an azimuthal angle of 0 deg has the FSS shape. This simulation was carried out some time ago, with a coarser grid and hence the frequency resolution is not as good as in other results shown here. Despite this, the correct spectral shapes are still captured. This lower Mach number case highlights the importance of the dynamics of the large-scale structures in noise generation and radiation. In Fig. 16, the noise radiated to the azimuthal angles ($\pm$90 deg) is also symmetric and close to data. Note the subtle variations in the spectral levels and shapes for the different azimuthal angles. At a polar angle of 120 deg, for example, the peak levels are higher by $\sim$3 dB at an azimuthal angle of 90 deg and by $\sim$5 dB at 180 deg compared with the level at the azimuthal angle of 0 deg. The peak frequency has also moved to lower values with increasing azimuthal angle. These trends are reflected in the LES results; the agreement for the absolute predictions over the resolved frequencies with data is also good, for both the round and bevel45 nozzles.

When the Mach number is increased to 1.0, the azimuthal effects of the beveled nozzle become more pronounced, due to the higher jet velocity. Figure 17 shows comparisons for this case; at polar angles of 110 and 120 deg, there is a $\sim$10 dB increase in the peak noise levels radiated to an azimuthal angle of 180 deg, when compared with the level at an azimuthal angle of 0 deg. Again, the magnitudes of this change, at different polar angles, are correctly predicted by LES. Attention is drawn to the fact that the simulation was repeated with the finer grid for this case; therefore, the range of resolved frequencies is substantially larger than for the $M = 0.6$ case.

Finally, we show a case (heated $M = 1.56$ jet) with significant broadband shock-associated noise, caused by the interaction of the turbulence with the shock-cell system, for the round and beveled nozzles. Narrowband data from the bevel45 nozzle are shown in Fig. 18 at an azimuthal angle of 0 deg; the predicted shock peak frequencies, as well as the levels, are very good at all the lower polar

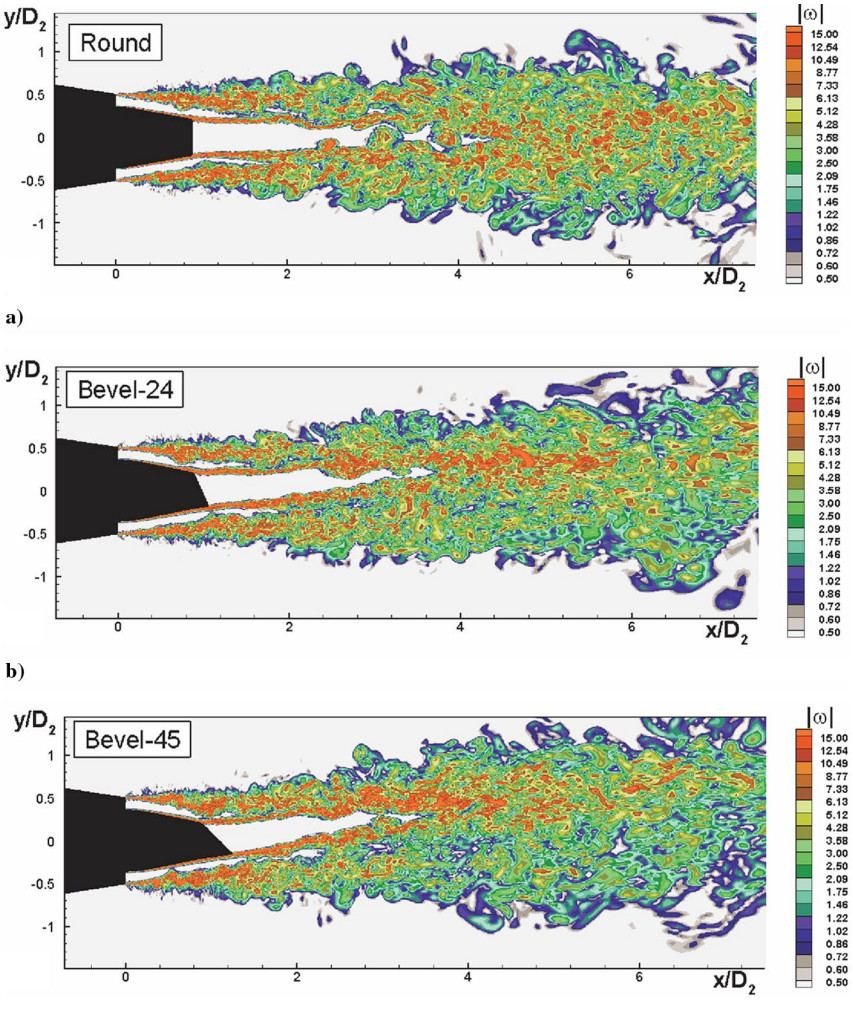

Fig. 21 Effect of primary nozzle beveling on snapshots of vorticity for the dual jets in still air.

angles, where shock-associated noise is dominant. Absolute predictions of the shock-noise peak locations and levels, without any empirical adjustments, attest to the validity of the approach and indicate that the right physics is captured in the simulations.

The directivities of overall sound pressure level (OASPL) for the round and bevel45 nozzles, at various azimuthal angles, are shown in Fig. 19. We notice in these figures that the predicted noise radiated to the sides ($\phi = \pm 90$ deg) by bevel45 is slightly higher than that for the round nozzle, a trend seen in the experiments. The predicted noise levels radiated to the azimuthal angle of 0 deg is lower than those at both 90 and 180 deg, again matching the experimental trends. In Fig. 19b, the noise benefit due to the bevel is negligible for $M = 0.6$. As the Mach number is increased to 1.0, the magnitude of the benefit is ~3 dB. At the highest Mach number of 1.56, the maximum benefit is ~8 dB at 130 deg. Further, the peak radiation angles are ~10 deg apart. These trends are reproduced in the simulations. At an azimuthal angle of 180 deg (Fig. 19c) the trends are reversed for the subsonic Mach numbers, with higher levels of noise for bevel45 at the lower polar angles; this trend is also captured in the predictions. Finally, the peak polar radiation angle moves to lower values at this azimuthal angle. The shift in the peak radiation angle by ~35 deg for $M = 1.56$ between $\phi = 0$ and $\phi = 180$ deg is captured well by the simulations.

D. Dual-Stream Nozzles

Exhaust geometries with dual-stream nozzles are ubiquitous in the commercial airplane industry and introduce additional complications for the numerical simulations. In many aircraft applications, the primary nozzle extends downstream of the fan nozzle; geometric features such as pylons, heat shields, struts, and bifurcations are still beyond the scope of the LES approach. Obviously, the grid requirements are much more demanding for two streams, because two shear layers must now be resolved. That is, the fine grid in the radial direction must be extended to a larger radial distance. This tends to require a finer resolution in the azimuthal direction as well. It is known that there is an elongation of the potential core for dual-stream jets, and a slower decay of turbulence in the axial direction. In the presence of a flight stream, the secondary shear layer also persists for a much longer distance because of the reduced shear; consequently, there is a substantial lengthening of the entire mixing region before the fully mixed state is reached. Therefore, the grids have to be finer in all three directions. Shur et al. [3] discuss the many issues and the steps taken to overcome them. An overview of the approach is provided here, before sample results are presented for conventional dual-stream geometry and ones with beveled primary nozzles.

Figure 20 shows a portion of the RANS grid for the dual-stream beveled nozzle; a close-up of the shear layers is also included. This grid is not adapted to the shear layers, which is acceptable because the focus is on inviscid effects, particularly inside the nozzles. The LES computational domains and the grids for the beveled nozzles are designed to account for the specific features of the flow, especially the plume deflection due to the beveled trailing edge. Similar to the practice adopted for the single beveled jet, the regions of fine radial grid are adjusted to the deflected shear layers. This adjustment is based on the findings in the RANS stage of the two-step computational procedure; proper grid design is necessary for an accurate representation of transition to turbulence. The region of fine axial grid is maintained in the extended area between the exits of the

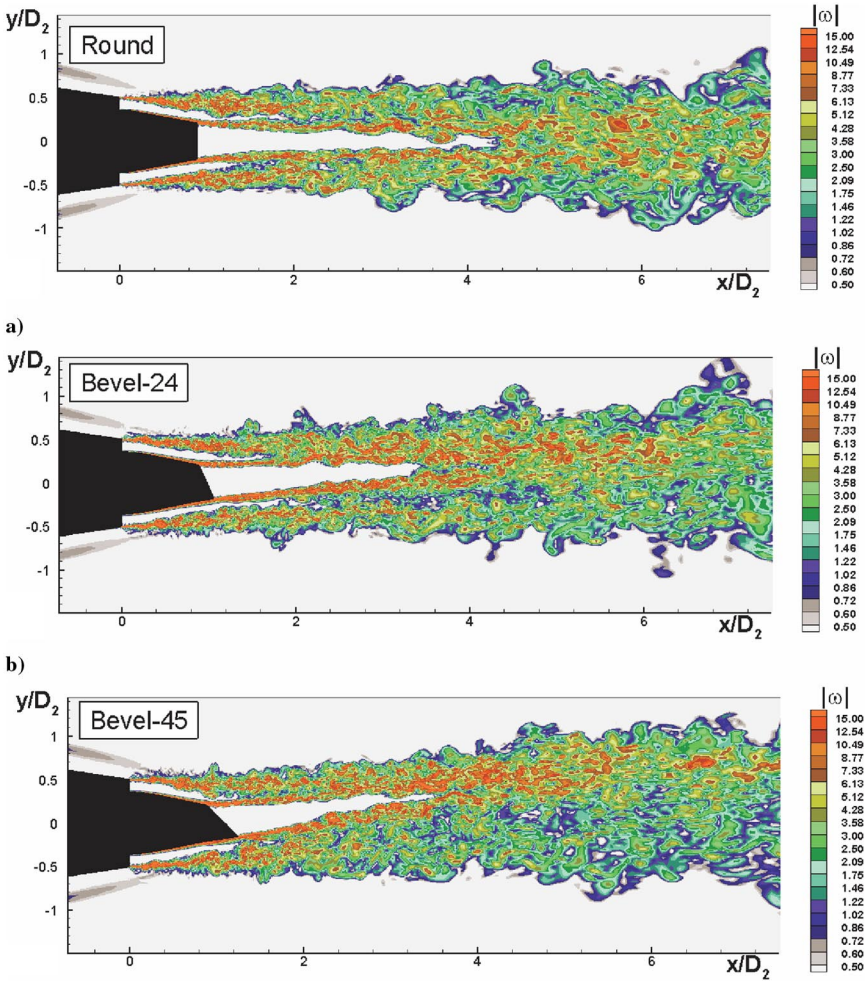

Fig. 22 Effect of primary nozzle beveling on snapshots of vorticity for the dual jets in flight conditions.

secondary and primary nozzles to ensure an acceptable resolution of the fan shear layer which is responsible for the generation of high-frequency noise; see [23] for more details. For jets in coflow, the region of fine axial grids is furthermore extended to a larger downstream distance to accommodate the elongation of the potential core due to the flight stream. This requirement necessitated an increase in the total number of grid points in the dual jets simulations up to ~4.5 million. The two-step approach of RANS/LES is adopted. The LES domain starts at the two staggered nozzle-exit planes. However, as discussed by Shur et al. [3], even this strategy is not fully adequate for these types of geometries. The external fan flow has a boundary-layer buildup on the outside of the primary nozzle. The primary and secondary nozzles are convergent; as a result, the outer boundary layers develop under adverse pressure gradients and streamline convergence. Both these effects thicken boundary layers. The implicit LES used for single jets and nonstaggered nozzles cannot treat turbulence in these boundary layers accurately, resulting in separation and vortex shedding. Again, an LES with wall modeling would be prohibitive computationally. The eddy viscosity is zero except in the boundary layer on the primary cowl; in this region, the RANS computations provide the values for the eddy viscosity. Therefore, a zonal strategy for the eddy viscosity, which keeps the boundary layer attached and provides fair noise predictions, was adopted; see [3] for more details.

A typical test case from the dual-stream database of Viswanathan [23] was chosen as follows: the nozzle pressure ratios for the primary and secondary streams are NPRp = NPRs = 1.8 and the temperature ratios are $Tp/Ta = 2.37$ and $Ts/Ta = 1.0$. The area ratio (As/Ap) for this nozzle is 3.0; the bypass ratio for this particular cycle condition is 4.7. Computations have been carried out for the static case, as well as with a flight stream, at $M_f = 0.2$, for the round and the two beveled primary nozzles, all with a common secondary nozzle. That is, there are three dual-stream nozzle exhaust geometries.

The effects of the bevel angle and those due to the flight stream on the flowfield are examined in detail. Instantaneous vorticity fields in the symmetry plane of the LES are presented for the three nozzle systems in Figs. 21 and 22 for the static and wind-on cases, respectively. Aside from the plume vectoring, there is significant alteration of the turbulence structure of the jets. For both the static and wind-on cases, the fan shear layers of the beveled nozzles are highly asymmetric with the "top" being narrower and the "bottom" substantially thicker than those for the round jets, after the top one begins merging with the core shear layer; this effect is much stronger for the bevel45 system. The fan flow needs to accommodate the upward deflection of the core stream, which stretches it on the upper side, resulting in this thinning of the shear layer; conversely, there is streamline convergence and thickening on the lower side. The narrowing of the top shear layer is more pronounced for the case with the flight stream for bevel45, with the outer shear layer completely filled with small intense vortices apparent in Fig. 22c. The modifications to the potential-core lengths are also highlighted by the vorticity fields:

1) As for the single jets, the length of the primary potential core is reduced as the bevel angle is increased.

2) The length of the secondary shear layer at the top is progressively shortened with increasing bevel angle.

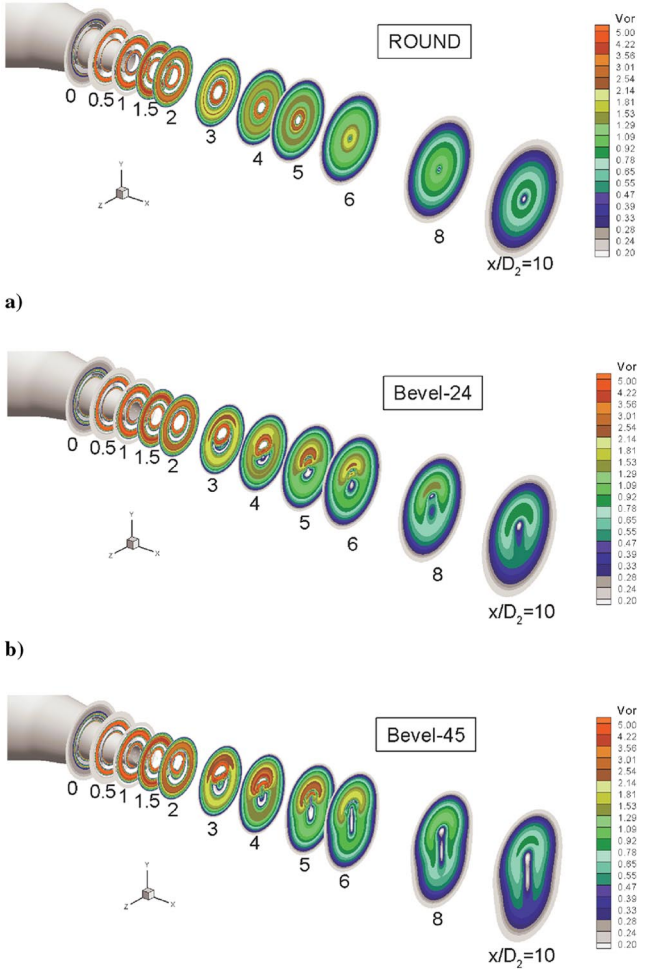

Fig. 23 Vorticity contours for the dual-stream jets at various cross sections. NPRp = NPRs = 1.8, $Tp/Ta = 2.37$, $Ts/Ta = 1.0$. a) round, b) bevel24, c) bevel45.

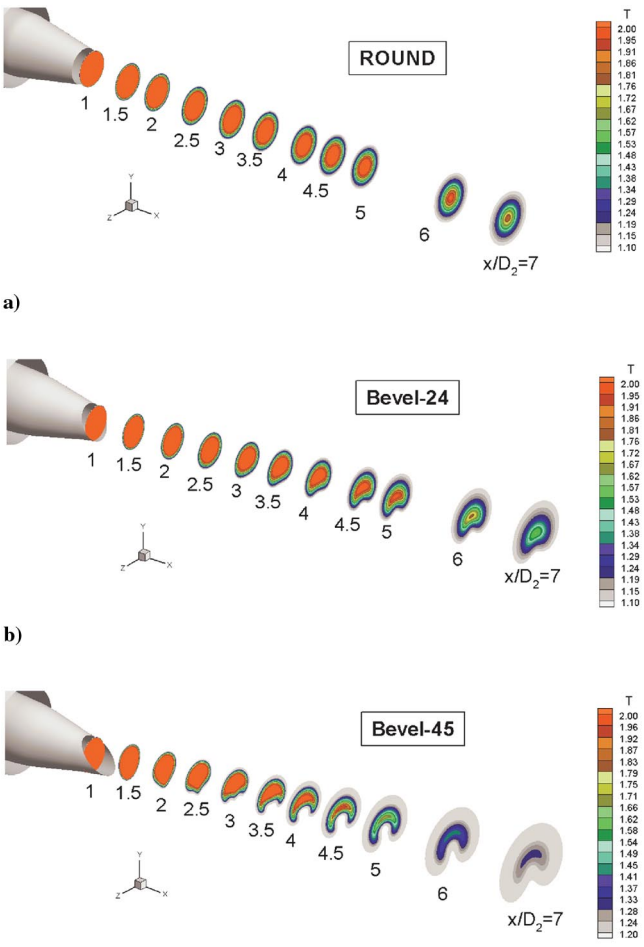

Fig. 24 Temperature contours for the dual-stream jets at various cross sections. NPRp = NPRs = 1.8, $Tp/Ta = 2.37$, $Ts/Ta = 1.0$. a) round, b) bevel24, c) bevel45.

3) The behavior of the bottom shear layer is different for the two beveled nozzles; it is somewhat longer than the round for bevel24, and shorter than the round for bevel45 due to the rapid widening of the outer shear layer.

In the preceding description, the secondary potential core is defined as the flow area between the two streams, free of vortical structures.

An examination of the instantaneous vertical-velocity fields (not shown) for both the single and dual-stream bevels reveals the presence of an extended region with high vertical velocity caused by the strong nonuniformity of the static pressure at the exit plane. The level of the vertical velocity, which determines the plume deflection angle, is strongly dependent on the bevel angle, but is almost insensitive to the presence or absence of the flight stream; it is sheltered by the fan flow. In general, the flight stream suppresses the spreading of the jet for all three geometries; however, its effect on the elongation of the potential core is much weaker for the beveled jets than for the round jets.

As noted in the Introduction, we seek an explanation for the experimentally observed trends in noise through the examination of the flowfield. An attempt is made to establish some link between the measured modifications to the noise field by the bevel to the alteration of some flow features, through the following figures. It will be shown later that the predicted noise is in good agreement with the measured trends; otherwise, there is no justification for this exercise. If such a link were determined, it would be possible to arrive at a preliminary estimate for the optimal bevel angle on the basis of low-cost RANS computations alone. Of course, this is a daunting task. Before we present results from time-averaged LES, it is illustrative to examine the RANS fields to get an overall understanding of the flow behavior.

Several interesting features are observed when the cross-sectional contours of vorticity and temperature from the RANS computations at several axial stations are examined for the static case in Figs. 23 and 24, respectively. For the conventional nozzle, there are, of course, concentric rings of vorticity, mainly concentrated in the shear layers in the early mixing layers. As the flow evolves, these get gradually mixed out but retain their axisymmetric shape at all downstream locations. For the beveled nozzles, the region of high-vorticity migrates toward the shorter side of the beveled nozzle and the plume gets elongated in the vertical plane. The fan flow (mixed with the ambient air) gets pulled toward the center of the core jet and the primary shear layer takes on a "C" shape; this trend is more vividly displayed in the cross-sectional plots of temperature in Fig. 24. The secondary shear layer is highly asymmetric, much thicker at the bottom, as also seen in the plots of instantaneous vorticity from the LES in Figs. 21 and 22.

The distributions of the mean axial and radial (or vertical) velocities, and the jet temperature in the jet's symmetry plane ($z = 0$), are shown in Figs. 25–27, respectively. In this and the following figures, round-jet results were not symmetrized, which has the value of giving the reader an idea of the remaining statistical scatter. This scatter is deemed to reflect a reasonable compromise, for a given computing budget, between smoothness and the breadth of the set of cases that have been treated. The static and wind-on cases are shown side-by-side to highlight the effects of the flight stream on the flow. For the baseline case, the end of the potential core (based on axial velocity) is $\sim 4.5D_2$. For the beveled nozzles, there is asymmetric mixing and the primary shear layer reaches the outer shear layer closer to the nozzle. This aspect of the flow is obvious in the temperature distribution plots. The normal velocity reaches a value of $\sim 12\%$ of the axial jet velocity for the bevel45 and there is a large region where the values remain high. Note that the effect of the flight stream on the vertical-velocity field is negligible. As expected, the plume deflection angle is also higher for the bevel45. There is a shortening of the primary potential core for both beveled nozzles.

Comparisons of the profiles of the mean streamwise velocity in the symmetry plane ($z = 0$) at several axial stations are shown in Fig. 28 for the wind-on case. The secondary shear layer rapidly gets mixed out and the peak velocity regions migrate toward the shorter lip of the beveled nozzle, denoted by positive y values. Similar trends are observed for the static case (not shown). The distributions of the

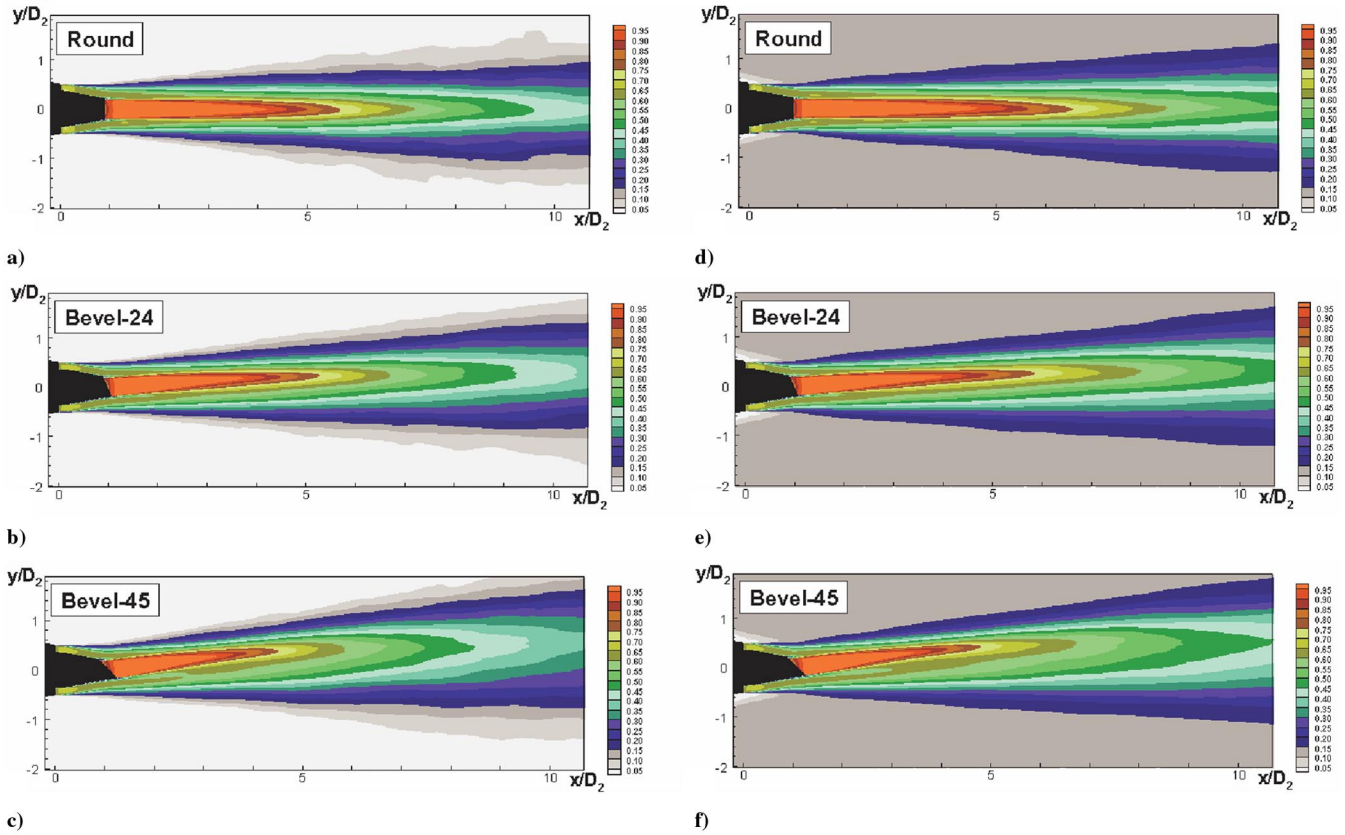

Fig. 25 Mean axial velocity U/U_p contours in the jet's symmetry plane. NPRp = NPRs = 1.8, Tp/Ta = 2.37, Ts/Ta = 1.0. a–c) still air, d–f) wind-on case.

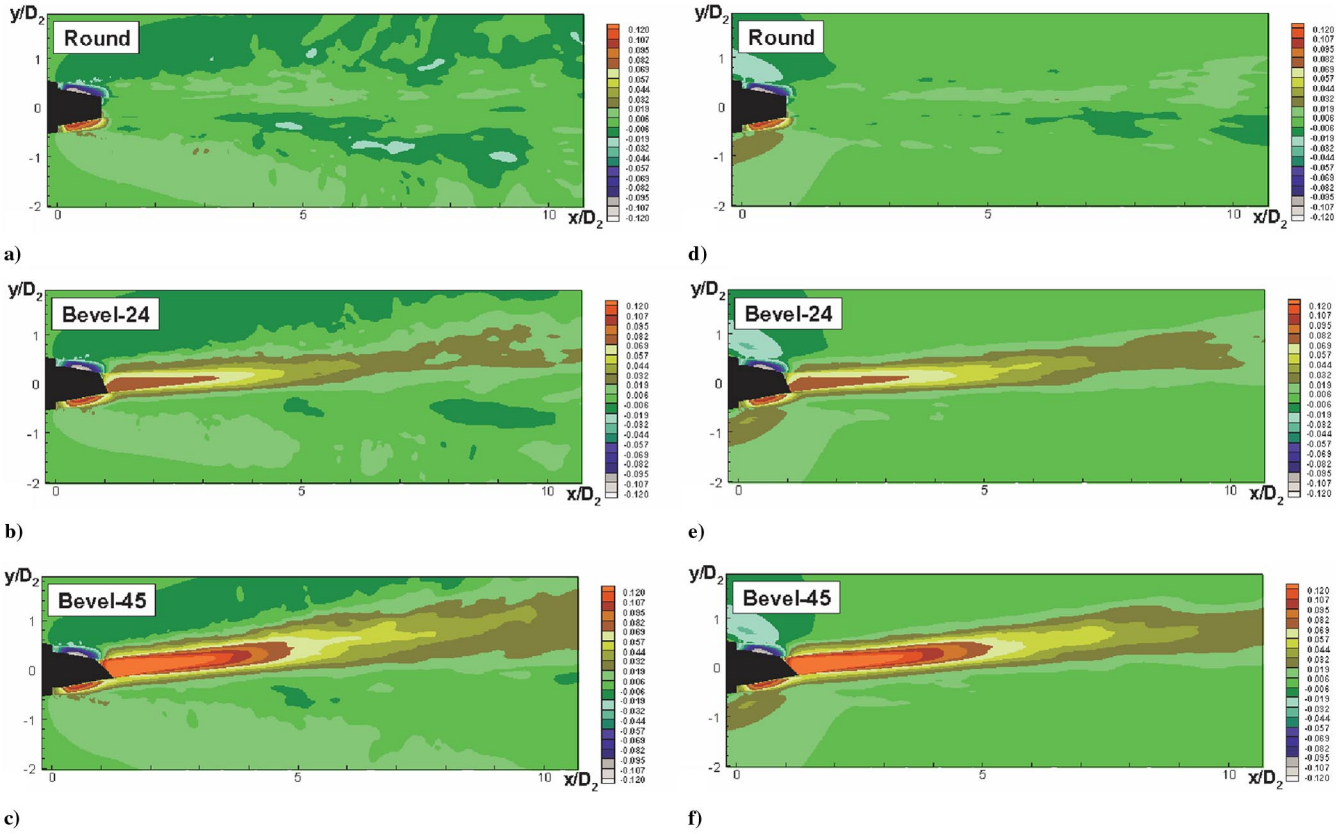

Fig. 26 Mean vertical velocity V/U_p contours in the jet's symmetry plane. NPRp = NPRs = 1.8, Tp/Ta = 2.37, Ts/Ta = 1.0. a–c) still air, d–f) wind-on case.

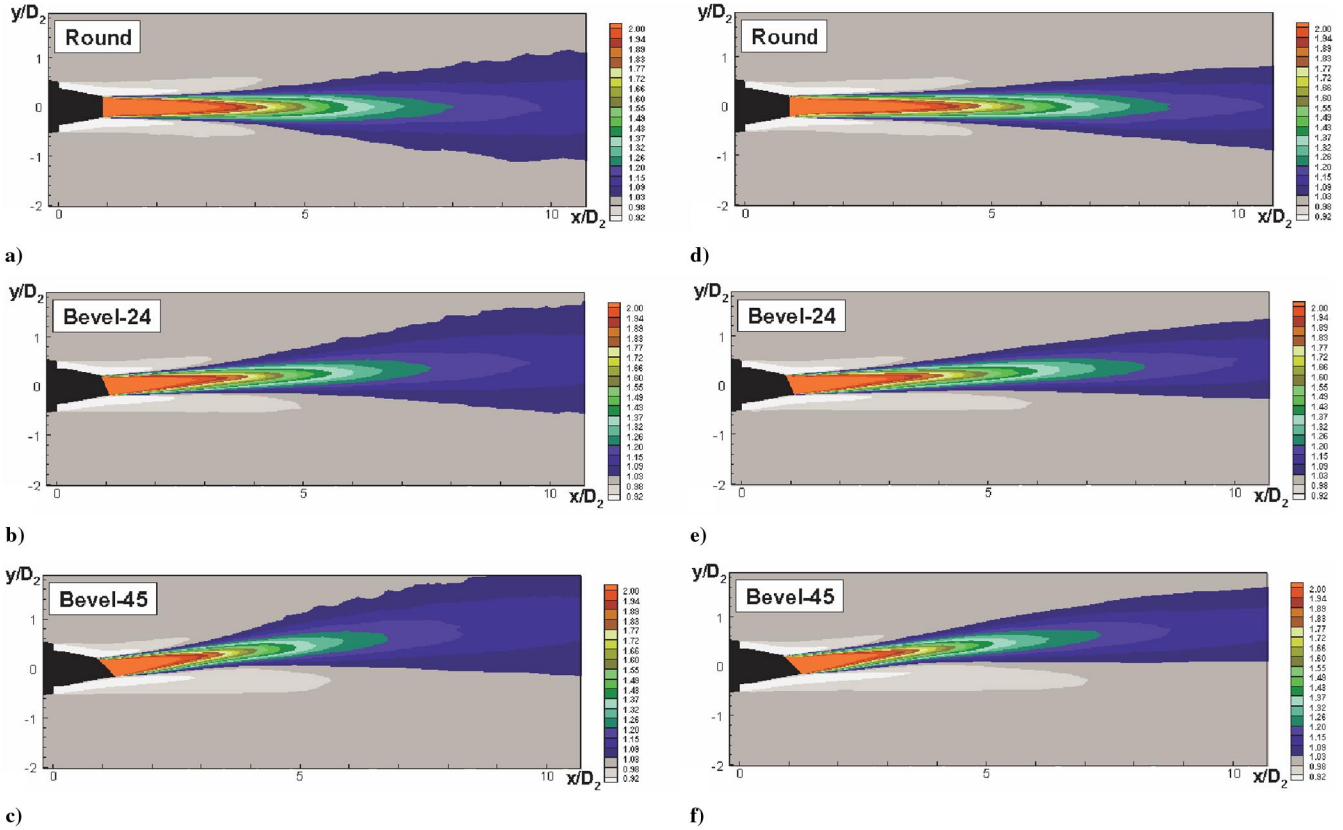

Fig. 27 Mean temperature T/T_a contours in the jet's symmetry plane. NPRp = NPRs = 1.8, Tp/Ta = 2.37, Ts/Ta = 1.0. a–c) still air, d–f) wind-on case.

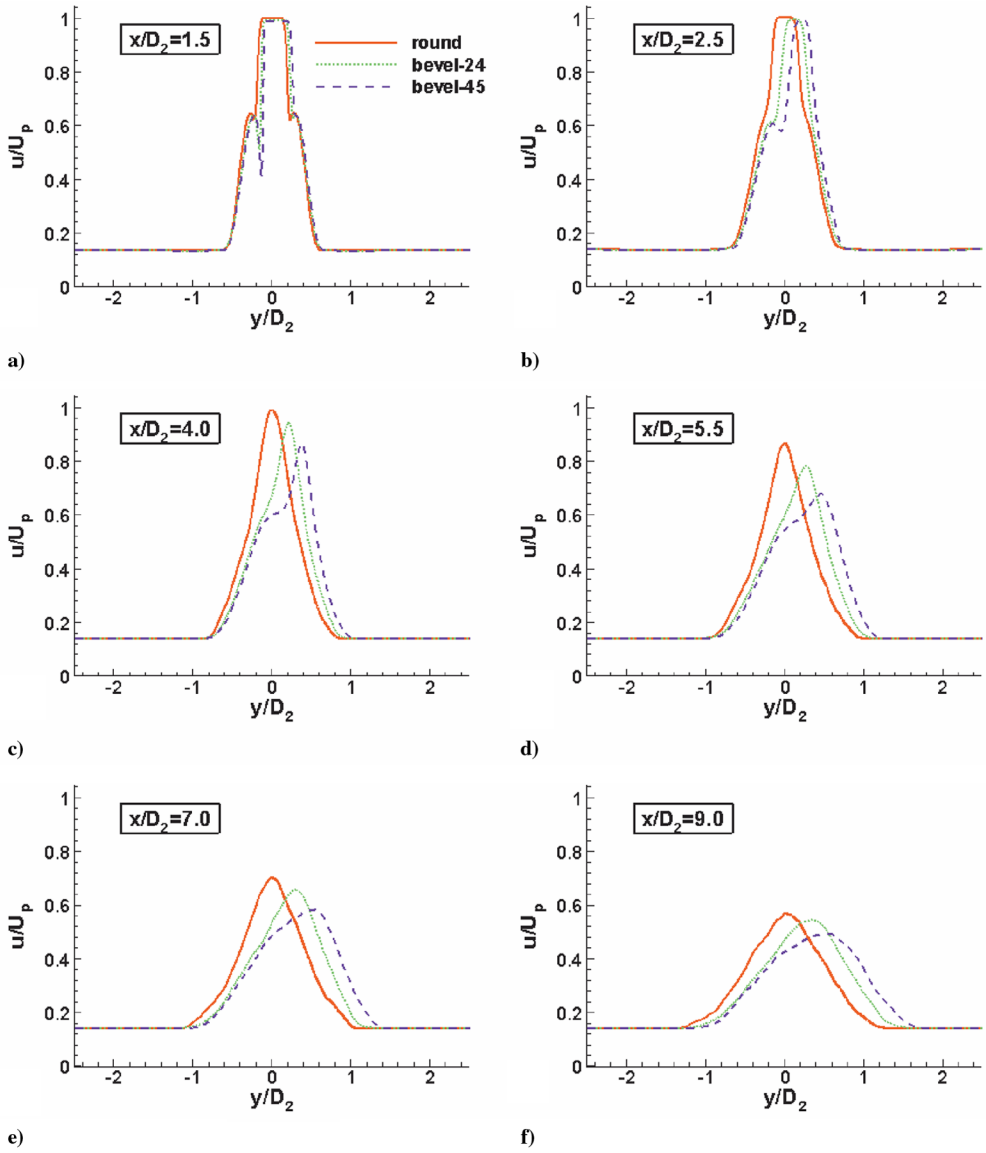

Fig. 28 Effect of primary nozzle beveling on profiles of the mean axial velocity in the jet symmetry plane $z = 0$ for the wind-on case.

turbulent kinetic energy (TKE) for the three geometries are shown in Fig. 29. There is a significant effect of the nozzle beveling on the magnitude and the distribution of TKE; a striking feature is the noticeable increase in the TKE level, which monotonically increases in the upper shear layer. There is a commensurate reduction in TKE in the lower shear layer, a trend observed for both the static and wind-on cases, and a favorable indication regarding noise radiated toward the ground. The variations of the maximum levels of TKE in the symmetry plane, which occur at different axial locations, are shown in Fig. 30. First of all, there seems to be a lower limit at the bottom shear layer, because the levels are the same for both the beveled nozzles. There is a substantial increase of $\sim$8% for the bevel45 at the top shear layer. Finally the profiles of $|\partial U/\partial y|$ in the symmetry plane, at the axial locations where TKE reaches its maximum, are depicted in Fig. 31. Again, the asymmetric distributions for the beveled nozzles exhibit higher levels at the top shear layer and substantially lower values in the lower shear layer.

It is obvious that there are substantial differences in the development of the mean and turbulence fields for the beveled nozzles. Quantities such as TKE and $|\partial U/\partial y|$ are associated with source terms in theories of jet noise. However, it is not obvious how the observed differences in the distributions of these parameters between the round and beveled nozzle systems relate to the differences in the radiated noise fields.

The acoustic characteristics from the LES are examined next. There are subtle variations in the measured noise spectra; the ability of LES to capture these trends is established with the following figures. It will be recalled that due to time constraints during the test, no measurements were made at an azimuthal angle of 180 deg, toward the shorter lip of the beveled nozzles. The results from the simulations help to fill this void.

Figures 32 and 33 show snapshots of $(\partial p/\partial t)$ for the three nozzle systems; the static and wind-on cases are depicted, respectively. There is a well-defined peak sector of radiation in the aft direction, with a noticeable reduction of the downward radiated noise for the beveled nozzles compared with the round nozzle. The introduction of the flight stream results in a reduction of the intensity of radiation (note that the same scale for the contours is used for the two cases). This effect has been measured in wind-tunnel tests and the simulations capture this trend. A surprising result is that the upward radiated noise is significantly higher than the downward levels for the beveled nozzles. This trend is vastly different from that observed for the single beveled jet, for which the upward and downward radiated noise in the peak directions were both lower than the levels for the round nozzle.

This observation is reinforced and quantified in the directivity plots shown in Figs. 34 and 35 for the static and wind-on cases. The magnitude of the noise reduction in the peak radiation sector

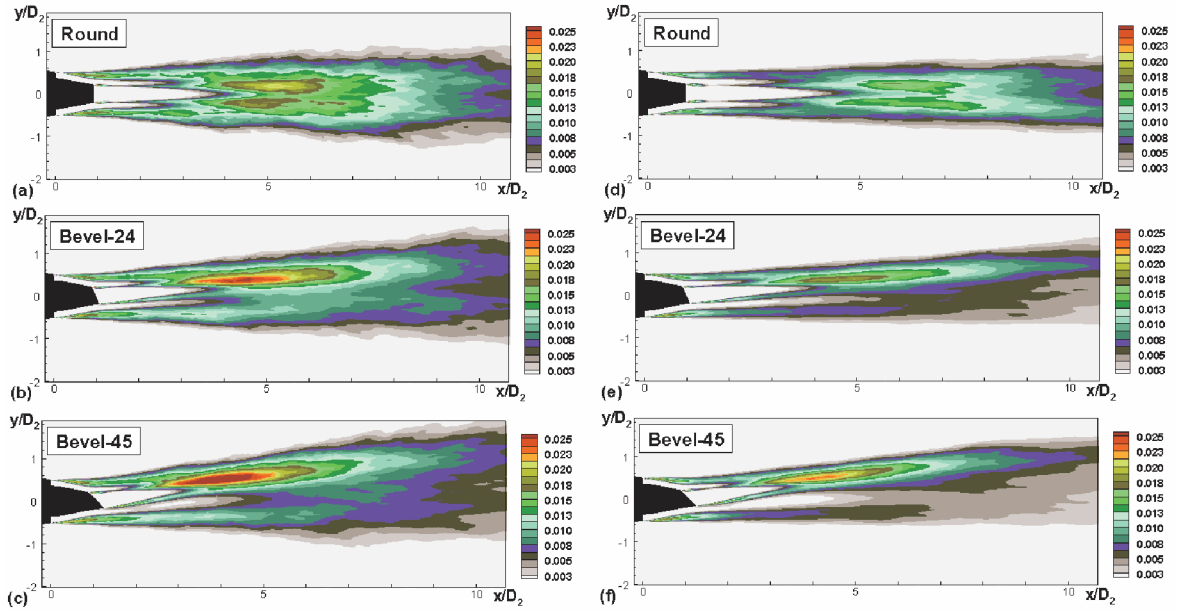

Fig. 29 Resolved turbulent kinetic energy k_t/U_p^2 contours in the jet's symmetry plane. NPRp = NPRs = 1.8, Tp/Ta = 2.37, Ts/Ta = 1.0. a–c) still air, d–f) wind-on case.

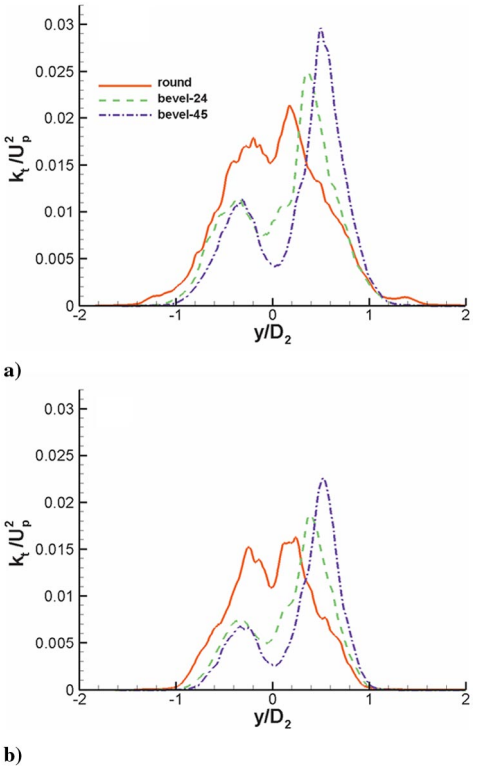

Fig. 30 Effect of primary nozzle beveling on profiles of resolved turbulent kinetic energy in jet's symmetry plane at x stations where TKE reaches its maximum. a) still air (x/D_2 = 5.3, 4.5, and 4.0 for round, bevel24, and bevel45 nozzles, respectively); b) wind-on case (x/D_2 = 6.0, 5.0, and 4.3).

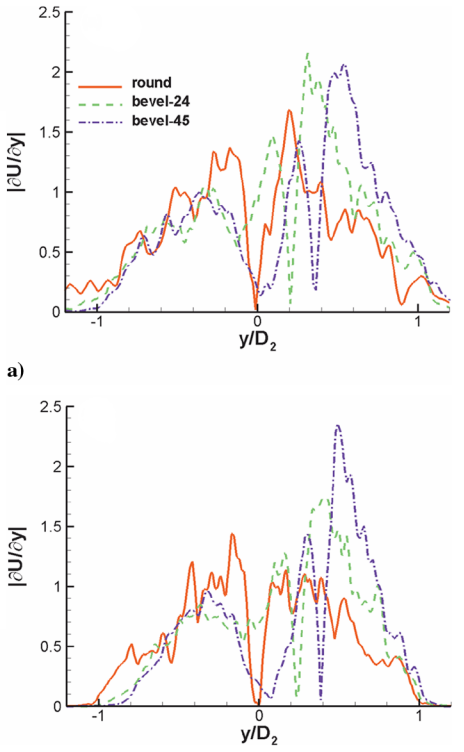

Fig. 31 Effect of primary nozzle beveling on profiles of $|\partial U/\partial y|$ in jet's symmetry plane at x stations where TKE reaches its maximum. a) still air, b) wind-on case. Same x stations as in Fig. 30.

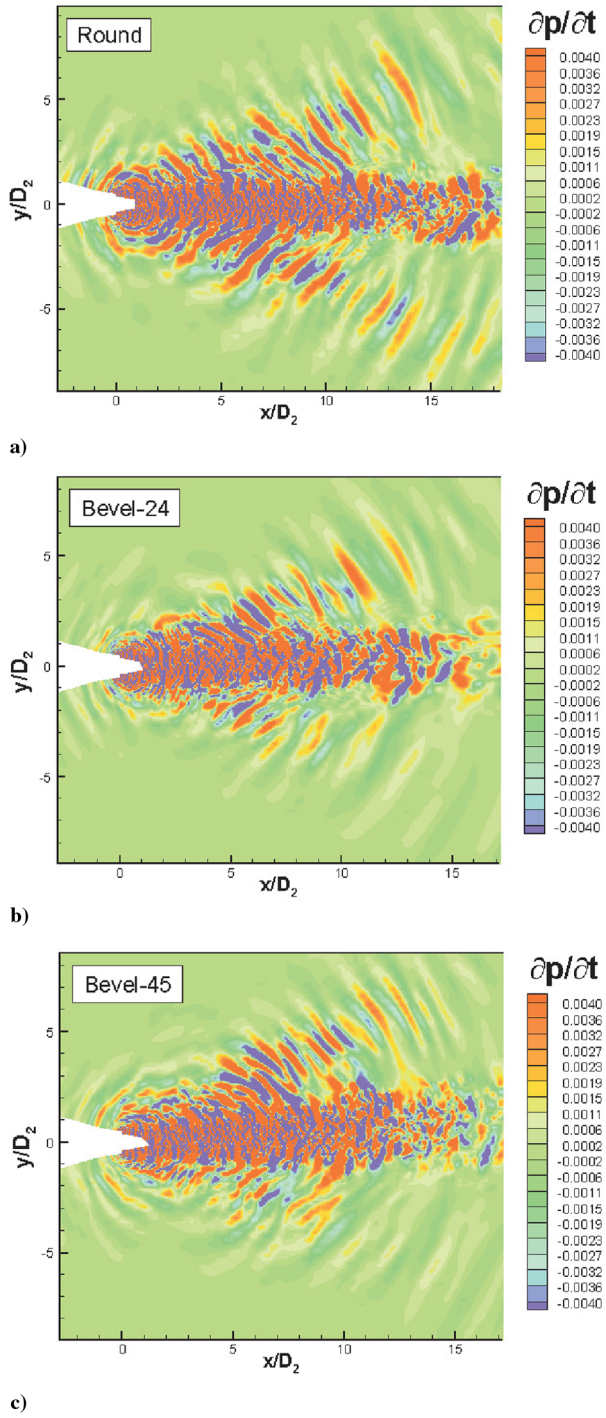

Fig. 32 Snapshots of the pressure-time derivative in the *XY* plane of symmetry. $Mf = 0.0$.

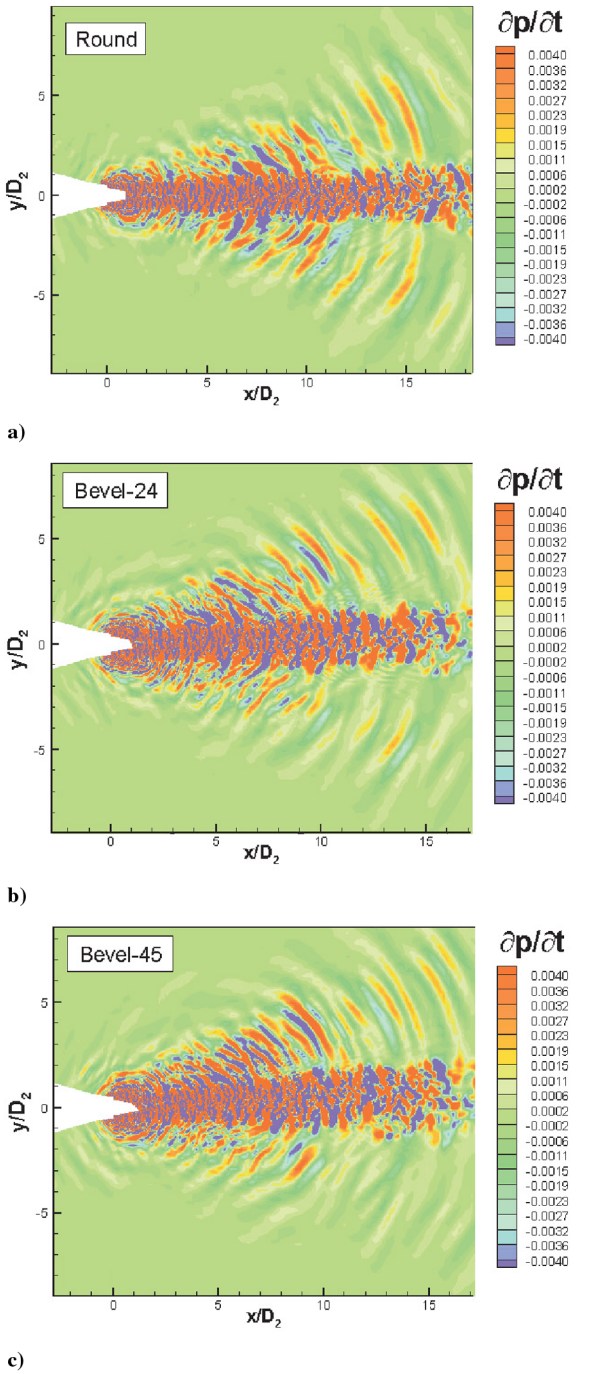

Fig. 33 Snapshots of the pressure-time derivative in the *XY* plane of symmetry. $Mf = 0.2$.

($> \sim 125$ deg) below the longer lip of the beveled nozzles is well predicted, though the absolute predictions are below the measured levels; this mismatch has been present in many of our simulations (see [2,3]). As noted in the $(\partial p/\partial t)$ snapshots, the upward levels are comparable to those from the round nozzle. Contrast this trend with that for the single nozzle in Fig. 19. Similarly, good agreement for the noise benefit at an azimuthal angle of 0 deg is predicted for the wind-on case. Thus, the predictions of the overall features are in good agreement with experimental data.

Finally, spectral comparisons are presented. Figure 36 shows comparisons with data for the baseline nozzle at static conditions; there is good agreement for the resolved range of frequencies, especially as we move to the aft angles. The LES line is stopped at a Strouhal number of $\sim$8.2, based on the fan-nozzle diameter and the fan-jet velocity. As noted in [23] though, there are several length and velocity scales (primary, secondary, mixed) for the dual-stream jets. Comparable results for the bevel24 nozzle at two azimuthal angles of 0 and 90 deg at static conditions are shown in Figs. 37 and 38, respectively. Again, there is very good agreement in the aft quadrant. Note that the spectral levels near the peak are $\sim$2 dB higher at the polar angles of 130 and 140 deg for the side radiation than the downward radiation; these subtle variations are captured in the simulations. Figure 39 shows the effect of the bevel45 system relative to the conventional nozzle in the downward direction (azimuthal angle of 0 deg) at four polar angles of 90, 130, 140, and 150 deg. The measurements indicate that the change in spectral levels due to beveling at the lower polar angles, up to $\sim$125 deg, is minimal. At 140 deg, there is a measured reduction of $\sim$5 dB at the peak, which is correctly predicted in the simulation. At 150 deg, the

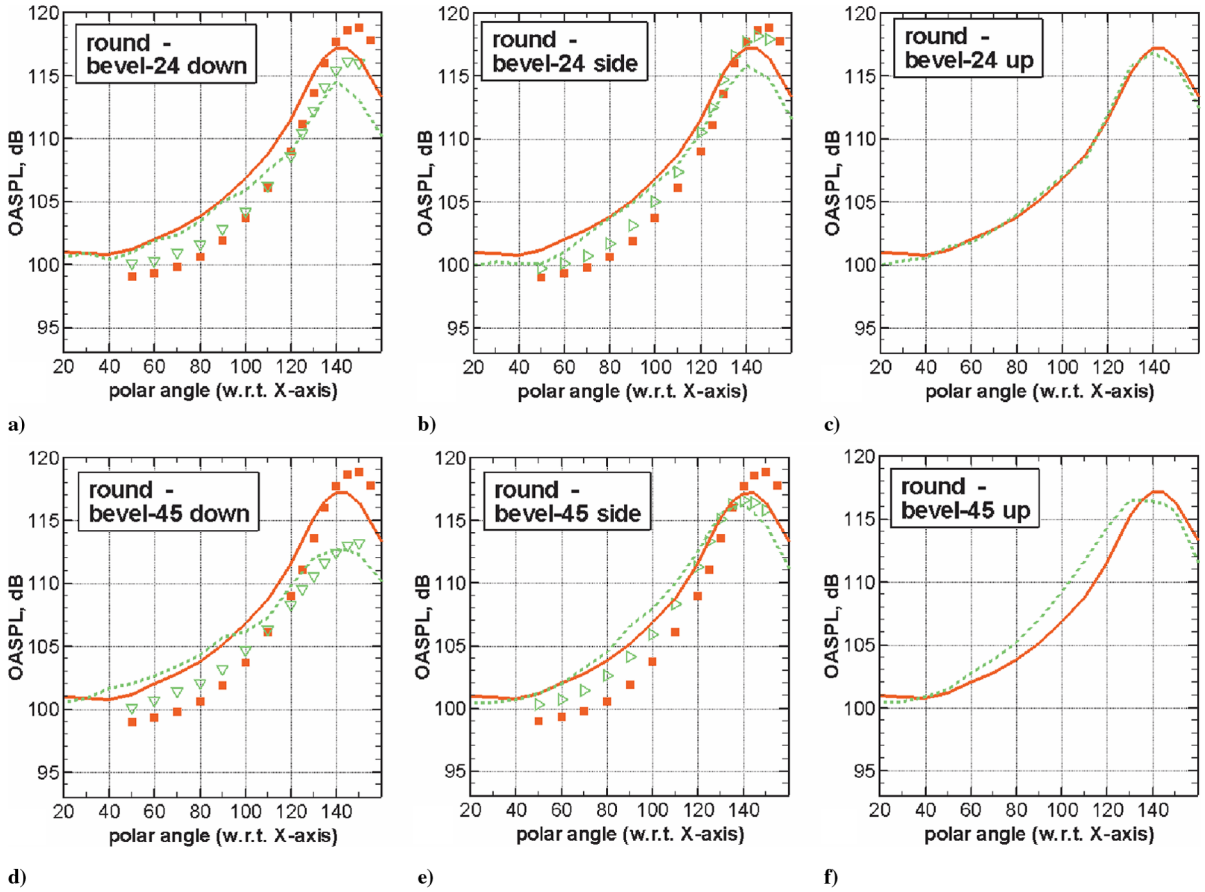

Fig. 34 Comparisons of OASPL directivities at various azimuthal angles for the jets in still air. NPRp = NPRs = 1.8, Tp/Ta = 2.37, Ts/Ta = 1.0. Filled symbols: round data; solid line: round LES; open symbols: bevel24 and bevel45 data; dashed line: bevel24 and bevel45 LES. a–c) bevel24; d–f) bevel45; a,d) azimuthal angle = 0 deg; b,e) azimuthal angle = 90 deg; c,f) azimuthal angle = 180 deg.

magnitude of the noise benefit increases further to ∼8 dB; again, the predictions match the data well. It is clear that there is a noise benefit at an azimuthal angle of 0 deg; however, the noise radiated to the side, at an azimuthal angle of 90 deg, exhibits some interesting features as shown in Fig. 40. First of all, there is a crossover with a noise benefit at the lower frequencies and a noise increase for the higher frequencies for the beveled nozzle. The measured spectra at polar angles of 90, 120, 130, and 140 deg indicate the magnitude of the noise increase at the higher frequencies to be ∼2 dB. The predicted spectra clearly exhibit the same trends. The azimuthal variation at a polar angle of 140 deg varies from a ∼5 dB noise benefit near the spectral peak in the downward direction to ∼1 dB noise benefit and a crossover to a noise increase in the sideward direction. The excellent agreement of the predictions with these trends attests to the accuracy of the numerical system.

Spectral comparisons for the wind-on cases are now presented at the polar angles of 90, 130, 140, and 150 deg in the downward direction in Figs. 41 and 42. The spectral shapes and the magnitudes of the noise change in the spectra are in good agreement with the experiments. In general, the spectral agreement is within ∼3 dB at most angles, with a closer agreement at many angles.

The observed better agreement in the aft angles could be due to the following reason. As noted in [14,23], the secondary shear layer is responsible for the generation of the high-frequency noise and the fully mixed jet generates most of the low-frequency noise radiated to all angles. The primary shear layer is responsible for the low- and midfrequency noise increase observed at aft angles. We have learned from our experience with single jets that it is important to have good grid resolution of the region downstream of the potential core, as well as the initial shear layer. The frequencies generated by the fan shear layer are beyond the maximum resolved frequency and beyond the capability of LES even on the most powerful available computer. For example, Figure A4 in [23] (reproduced here as Fig. 43) indicates that the secondary shear layer generates all the noise above a frequency of ∼15 kHz for the chosen cycle condition. This frequency is just above the limit of the current LES. Therefore, it might be possible to optimize the grid distribution in such a way that, for a given total number of grid points, the regions that produce the low- to midfrequency noise regions are adequately resolved. That is, the secondary shear layer can be sacrificed, within limits of course, because the noise from this source cannot be predicted anyway with the computers available to us. However, the shear layer is not properly resolved with too coarse a grid, resulting in the formation of large (nonphysical) vortices. This problem adversely affects the midfrequency noise predictions, with an overestimation in the near-normal directions. Thus, this approach requires a careful balance in the grid distribution: first and foremost, the flow must be adequately resolved. Additional grid points for this flow region would not necessarily increase the range of resolved frequencies.

As seen here for the single and dual-stream jets, a good knowledge of the important source regions of jet noise allows one to extend the range of resolved frequencies, as well as to obtain good spectral predictions. Attention is drawn to one specific example. In the spectral comparisons shown in Fig. 11, the number of grid points was roughly doubled: from ∼1.5 million to ∼2.9 million. In the common way of thinking, one would expect an increase in the frequency range by a factor of 1.26 (cube root of two). Yet, the range of the resolved frequency was almost doubled, from ∼1.35 to ∼2.7. This is a noteworthy achievement that highlights the crucial importance of efficient grid design and proper grid distribution.

IV. Summary

The flow and the noise characteristics of beveled nozzles have been investigated, with the goal of gaining insights into the flow features that are responsible for noise generation, which would

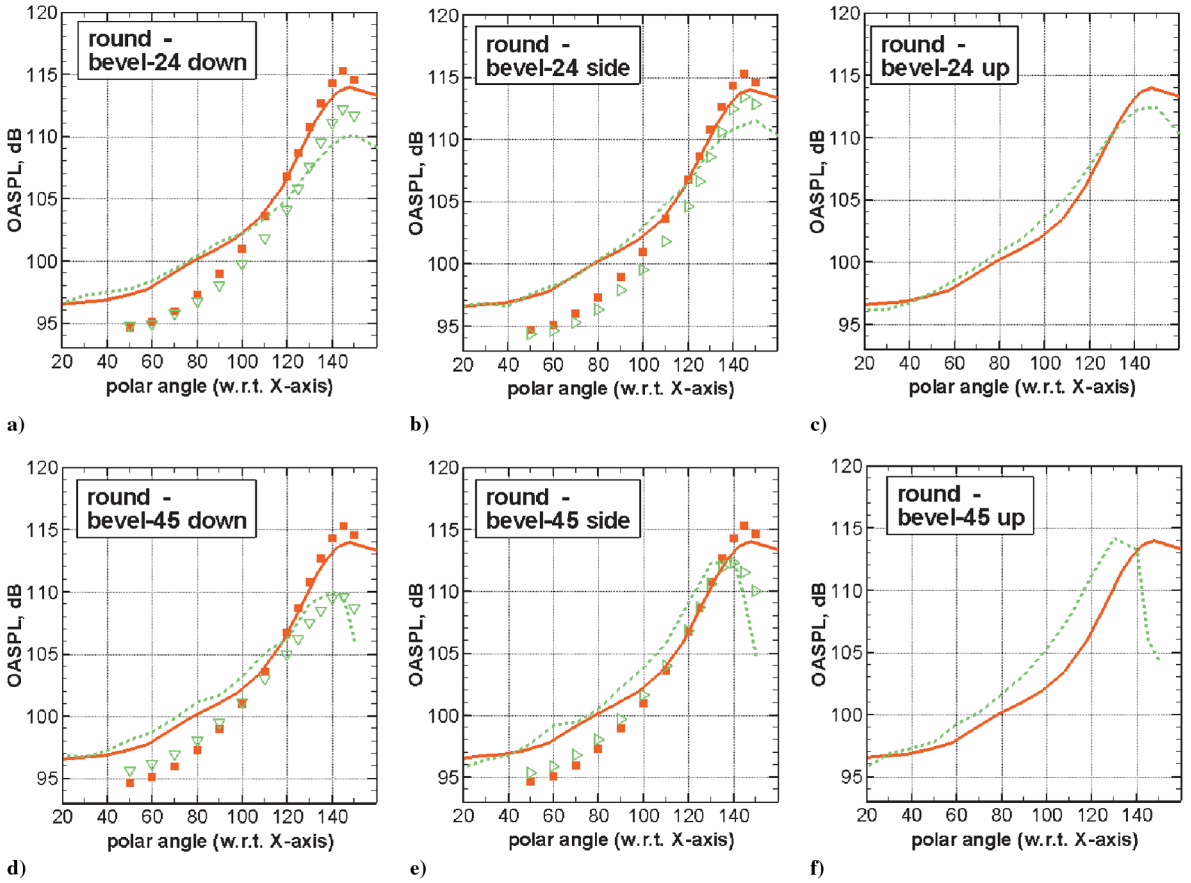

Fig. 35 Same as in Fig. 34, for the wind-on case.

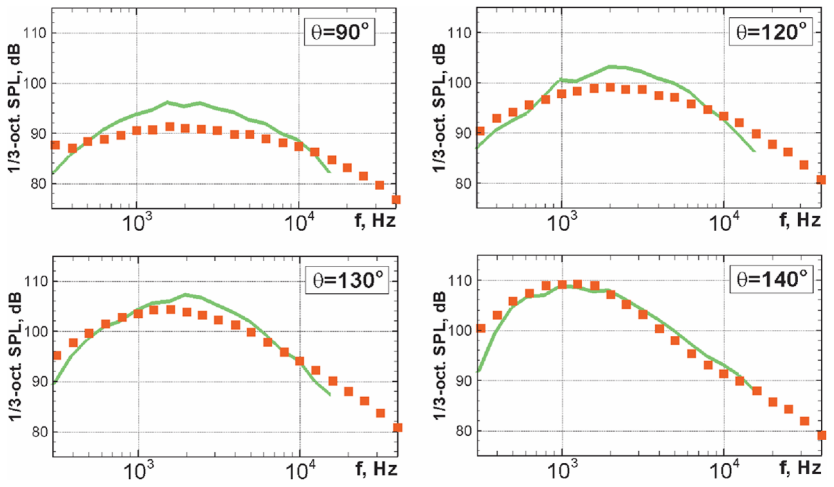

Fig. 36 Spectral comparisons from dual-stream round jet. NPRp = NPRs = 1.8, Tp/Ta = 2.37, Ts/Ta = 1.0.

perhaps lead to the determination of the optimum bevel angle for noise reduction. The importance of taking into account the nozzle internal flow, especially for complex geometries of interest and aircraft applications, has been emphasized once again; see [3,21]. A RANS simulation of the entire flowfield is first carried out; the RANS computations provide the inflow conditions, with adequate resolution of the boundary layers inside the nozzle. However, the important effects sought in the RANS for these conical beveled nozzles are inviscid. LES of the external plume is performed for noise prediction in the second step.

Based on detailed analyses of the measured spectra from beveled nozzles, it was concluded in [13,14] that the noise reduction achieved in the peak radiation sector in the aft quadrant is due to the alteration of the noise radiated by the large-scale turbulence structures in the flow. Large-eddy simulations have been carried out to understand the dynamics of the large-scale turbulence structures in noise generation for both round and beveled single and dual-stream nozzles. First of all, it is highlighted that good spectral agreement with measured data has been achieved for a wide range of jet operating conditions for both single and dual-stream nozzles; the effect of forward flight on noise has also been accurately predicted. Absolute predictions, without any empiricism, yield noise levels in most cases within ~2–3 dB of data. These good spectral predictions signify that the correct physics is captured and give us confidence that the interpretations of the flow/noise solutions are valid.

The LES predictions for the beveled nozzle capture the experimental trends; the predicted azimuthal variations in the spectra are in good agreement with the measured data. The jet plume is

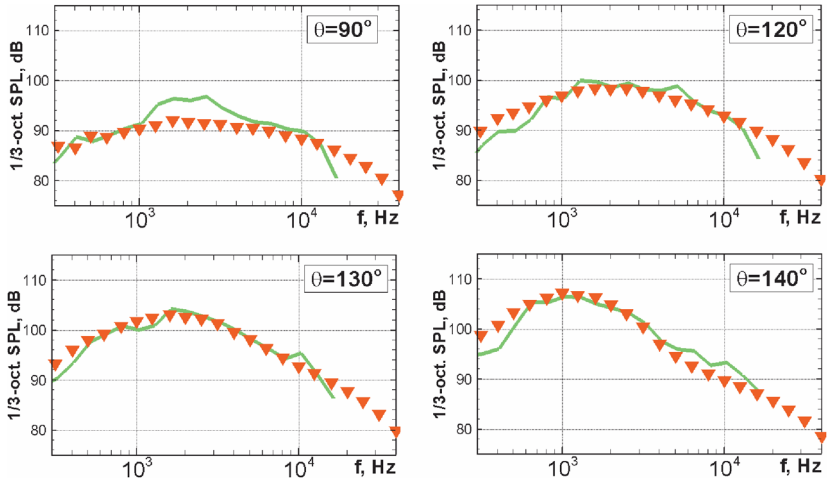

Fig. 37 Spectral comparisons from dual-stream bevel24 jet. NPRp = NPRs = 1.8, Tp/Ta = 2.37, Ts/Ta = 1.0. Azimuthal angle = 0 deg.

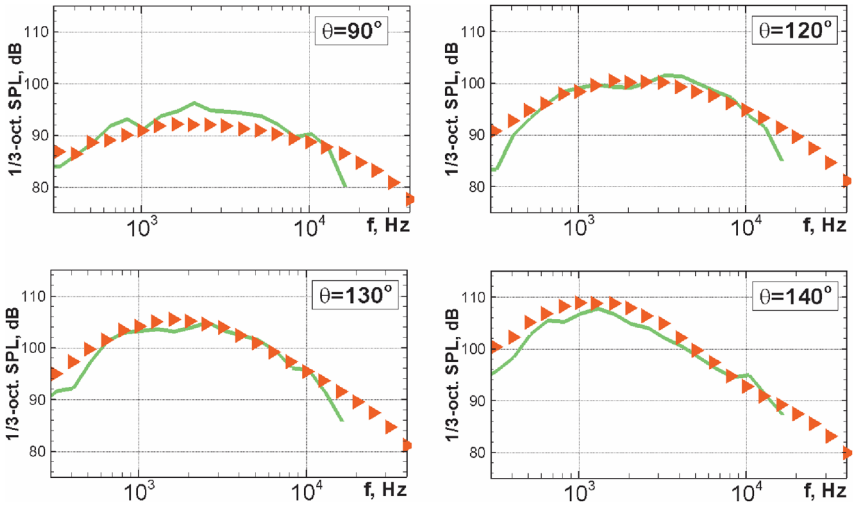

Fig. 38 Spectral comparisons from dual-stream bevel24 jet. NPRp = NPRs = 1.8, Tp/Ta = 2.37, Ts/Ta = 1.0. Azimuthal angle = 90 deg.

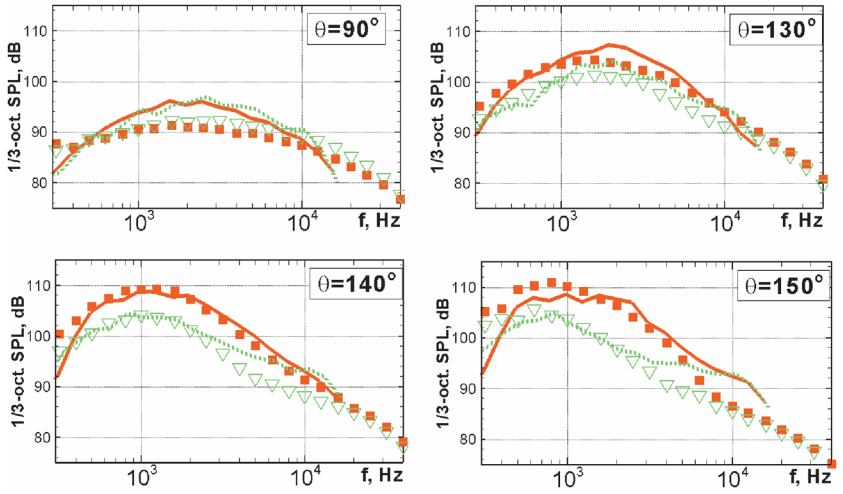

Fig. 39 Comparison of spectra between round and bevel45 nozzle systems. Mf = 0.0. Azimuthal angle = 0 deg. Symbols: experiment (filled: round; open: beveled); lines: LES (solid: round; dashed: beveled).

elongated in the direction of the symmetry plane and compressed in the other direction in the cross-sectional plane. The shift in the peak radiation to lower polar angles toward the shorter lip of the bevel is predicted well by LES. Excellent resolution of the broadband shock-associated noise for the beveled nozzle has also been demonstrated. The shock cells are damped out faster for the beveled nozzle. The mean-flow and turbulence fields are not too different between the round and beveled single nozzles, and there is nothing obvious that points to a reason for the noise reduction achieved with the single beveled nozzle.

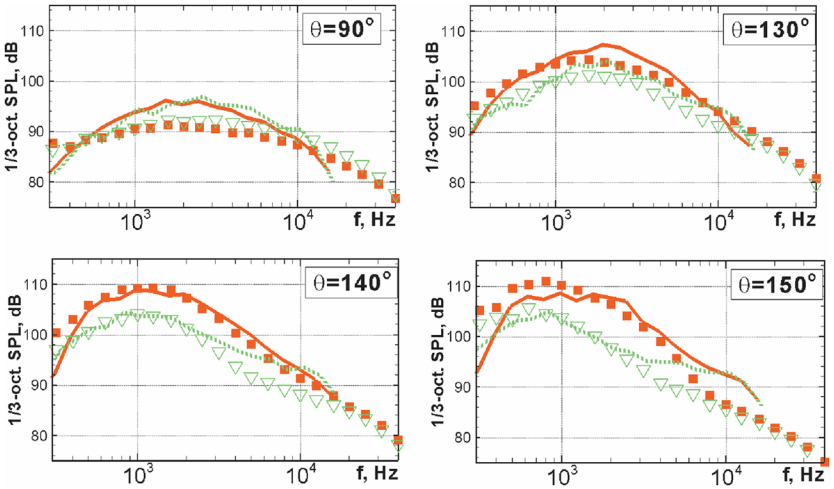

Fig. 40 Comparison of spectra between round and bevel45 nozzle systems. $Mf = 0.0$. Azimuthal angle = 90 deg. Symbols: experiment (filled: round; open: beveled); lines: LES (solid: round; dashed: beveled).

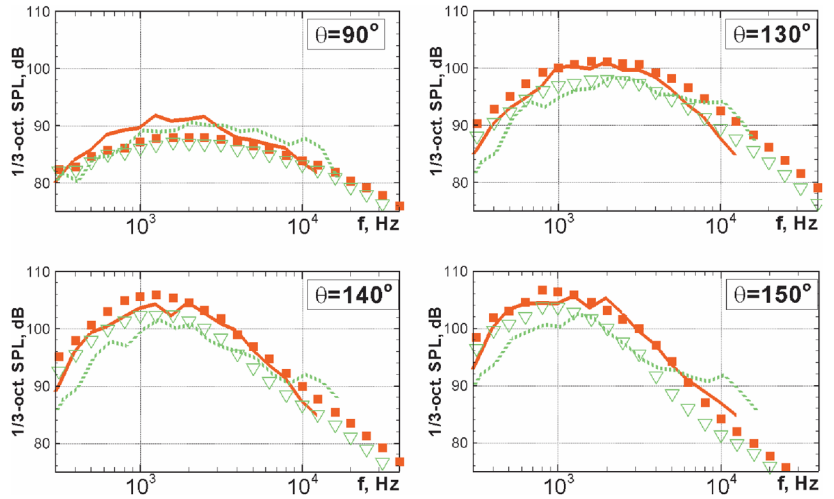

Fig. 41 Comparison of spectra between round and bevel24 nozzle systems. $Mf = 0.2$. Azimuthal angle = 0 deg. Symbols: experiment (filled: round; open: beveled); lines: LES (solid: round; dashed: beveled).

More attention has been given to the dual-stream exhaust systems with extended primary nozzles because of their practical relevance. The grid requirements are more severe for this geometry; the application of the hybrid RANS/LES methodology is also not straightforward. The importance of the grid topology and the efficient distribution of the grid points to achieve accurate noise predictions have been established for both the single and dual-stream nozzles. In spite of these complexities, good spectral predictions

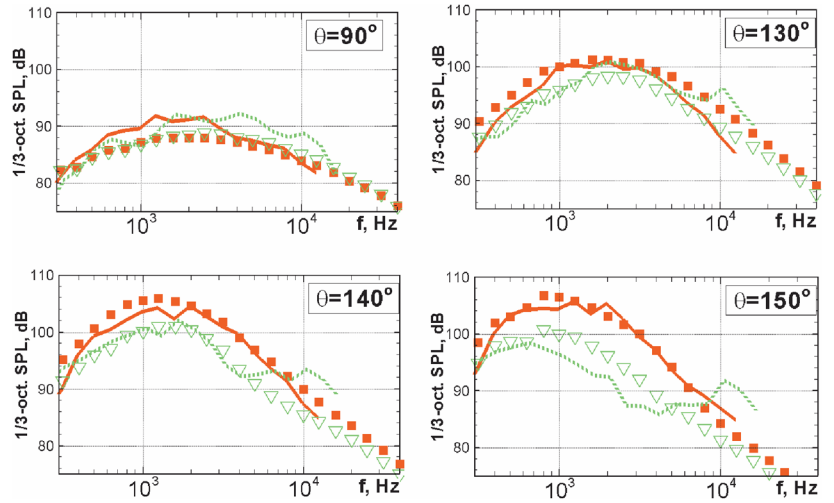

Fig. 42 Comparison of spectra between round and bevel45 nozzle systems. $Mf = 0.2$. Azimuthal angle = 0 deg. Symbols: experiment (filled: round; open: beveled); lines: LES (solid: round; dashed: beveled).

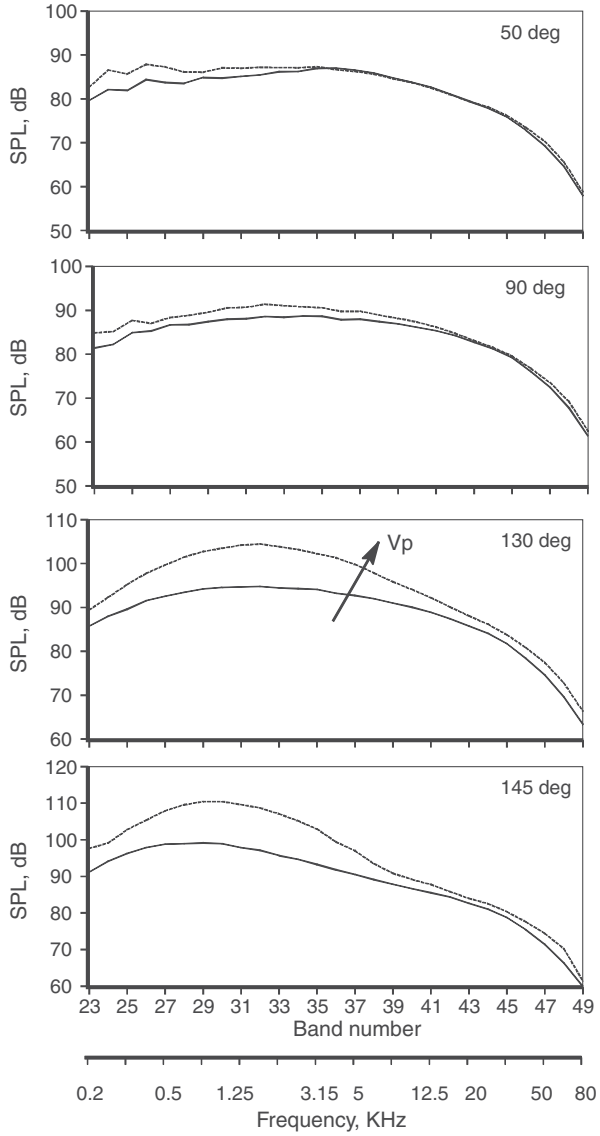

Fig. 43 Spectral variation due to change in primary stream with fixed secondary jet conditions. NPR$s = 1.8$, $Ts/Ta = 1.0$. Solid: NPR$p = 1.8$, $Tp/Ta = 1.0$; dashed: NPR$p = 1.8$, $Tp/Ta = 2.37$.

have been obtained for exhaust systems with both the round and beveled primary nozzles.

The mean-flow and turbulence fields for the beveled cases exhibit several interesting features and are quite different from those of the round nozzle. The fan shear layers are highly asymmetric with the top being narrower and the bottom substantially thicker than those for the round jets; this effect is much stronger for the bevel45 system. The lengths of the primary and secondary potential cores are altered consequently. The distributions of quantities that have been typically associated with noise sources are examined. The differences in the variations of TKE and $|\partial U/\partial y|$ between the round and bevel nozzle systems have been highlighted. In general, these quantities have much higher values in the top shear layer and are considerably lower in the lower shear layer. Concurrently, the far-field noise levels are lower toward the bottom direction. Because the noise received at an observer angle in the far field represents a summation from a distribution of sources (with possible cancellation) in the entire jet plume, it would probably be too simplistic to correlate the computed reductions in the "source" terms with the reduction in noise levels. The interpretation of the flow/noise connection is challenging and it is far from clear how one can establish cause and effect. The ability to relate changes in flow to noise will remain an open issue for the foreseeable future. LES can play an important role in this regard because the entire flow and noise fields are known, at least to some level of accuracy. This strong motivation drives our efforts in advancing the state of the art.

Acknowledgment

The authors from New Technologies and Services were partially supported by the Russian Basic Research Foundation, grant no. 06-08-00358.

References

[1] Shur, M. L., Spalart, P. S., and Strelets, M., "Noise Prediction for Increasingly Complex Jets, Part 1: Methods and Tests," *International Journal of Aeroacoustics*, Vol. 4, Nos. 3 and 4, 2005, pp. 213–246. doi:10.1260/1475472054771376

[2] Shur, M. L., Spalart, P. S., and Strelets, M., "Noise Prediction for Increasingly Complex jets, Part 2: Applications," *International Journal of Aeroacoustics*, Vol. 4, Nos. 3 and 4, 2005, pp. 247–266. doi:10.1260/1475472054771385

[3] Shur, M. L., Spalart, P. S., Strelets, M., and Garbaruk, A. V., "Further Steps in LES-Based Noise Prediction for Complex Jets," AIAA Paper 2006-485, Jan. 2006.

[4] Bogey, C., and Bailly, C., "Investigation of Subsonic Jet Noise Using LES: Mach and Reynolds Number Effects," AIAA Paper 2004-3023, May 2004.

[5] Bogey, C., Bailly, C., and Juve, D., "Noise Investigation of a High Subsonic, Moderate Reynolds Number Jet Using a Compressible LES," *Theoretical and Computational Fluid Dynamics*, Vol. 16, No. 4, 2003, pp. 273–297. doi:10.1007/s00162-002-0079-4

[6] Andersson, N., Eriksson, L. E., and Davidson, L., "Large Eddy Simulation of Subsonic Turbulent Jets and Their Radiated Sound," *AIAA Journal*, Vol. 43, No. 9, 2005, pp. 1899–1912.

[7] Bodony, D. J., and Lele, S. K., "Review of the Current Status of Jet Noise Predictions Using Large-Eddy Simulation," AIAA Paper 2006-486, Jan. 2006.

[8] Uzun, A., Lyrintzis, A. S., and Blaisdell, G. A., "Coupling of Integral Acoustics Methods with LES for Jet Noise Prediction," *International Journal of Aeroacoustics*, Vol. 3, No. 4, 2004, pp. 297–346. doi:10.1260/1475472043499290

[9] Paliath, U., and Morris, P. J., "Prediction of Noise From Jets With Different Nozzle Geometries," AIAA Paper 2004-3026, May 2004.

[10] Paliath, U., and Morris, P. J., "Prediction of Jet Noise from Circular Beveled Nozzles," AIAA Paper 2005-3096, May 2005.

[11] Rahier, G., Prieur, J., Vuillot, F., Lupoglazoff, N., and Biancheirn, A., "Investigation of Integral Surface Formulations for Acoustic Post-Processing of Unsteady Aerodynamic Jet Simulations," *Aerospace Science and Technology*, Vol. 8, No. 6, Sept. 2004, pp. 453–467. doi:10.1016/j.ast.2004.04.005

[12] Vuillemin, A., Loheac, P., Rahier, G., Vuillot, F., and Lupoglazoff, N., "Aeroacoustic Numerical Method Assessment for a Double Stream Nozzle," AIAA Paper 2005-3043, May 2005.

[13] Viswanathan, K., "Nozzle Shaping for Reduction of Jet Noise from Single Jets," *AIAA Journal*, Vol. 43, No. 5, 2005, pp. 1008–1022.

[14] Viswanathan, K., "Elegant Concept for Reduction of Jet Noise from Turbofan Engines," *Journal of Aircraft*, Vol. 43, No. 3, May–June 2006, pp. 616–626.

[15] Viswanathan, K., "Noise of Dual-Stream Beveled Nozzles at Supercritical Pressure Ratios," *Journal of Aircraft*, Vol. 43, No. 3, May–June 2006, pp. 627–638.

[16] Strelets, M. K., "Detached Eddy Simulation of Massively Separated Flows," AIAA Paper 2001-0879, Jan. 2001.

[17] Ffowcs Williams, J. E., and Hawkings, D. L., "Sound Generated by Turbulence and Surfaces in Unsteady Motion," *Philosophical Transactions of the Royal Society of London, Series A: Mathematical and Physical Sciences*, Vol. 264, No. 1151, 1969, 321–342. doi:10.1098/rsta.1969.0031

[18] Gulyaev, A. N., Kozlov, V. E., and Secundov, A. N., "Universal One-Equation Model for Turbulent Viscosity," *Fluid Dynamics*, Vol. 28, No. 4, 1993, pp. 485–494. doi:10.1007/BF01342683

[19] Shur, M., Strelets, M., Zaikov, L., Gulyaev, A., Kozlov, V., and Secundov, A., "Comparative Numerical Testing of One- and Two-Equation Turbulence Models for Flows with Separation and Reattachment," AIAA Paper 1995-0863, Jan. 1995.

[20] Spalart, P. R., Shur, M., Wright, M. C. M., and Morfey, C. L., "Variants of the Ffowcs Williams–Hawkings Equation with Favourable

Properties for Coupling with Turbulence Simulations," *Journal of Fluid Mechanics* (to be published), 2008.
[21] Viswanathan, K., Shur, M., Spalart, P. R., and Strelets, M., "Comparisons Between Experiment and Large-Eddy Simulation for Jet Noise," *AIAA Journal*, Vol. 45, No. 8, 2007, pp. 1952–1966. doi:10.2514/1.25892
[22] Tam, C. K. W., Golebiowski, M., and Seiner, J. M., "On the Two Components of Turbulent Mixing Noise from Supersonic Jets," AIAA Paper 96-1716, 1996.
[23] Viswanathan, K., "Parametric Study of Noise from Dual-Stream Nozzles," *Journal of Fluid Mechanics*, Vol. 521, 2004, pp. 35–68. doi:10.1017/S0022112004000813

C. Bailly
Associate Editor